The Astrophysical Journal, 591:1110–1128, 2003 July 10

SPECTROPOLARIMETRY OF SN 2001el IN NGC 1448: ASPHERICITY OF A NORMAL TYPE Ia SUPERNOVA[1]

Lifan Wang,[2] Dietrich Baade,[3] Peter Höflich,[4] Alexei Khokhlov,[5] J. Craig Wheeler,[4] D. Kasen,[2] Peter E. Nugent,[2] Saul Perlmutter,[2] Claes Fransson,[6] and Peter Lundqvist[6]

Received 2002 June 21; accepted 2003 March 10

ABSTRACT

High-quality spectropolarimetry (range 417–860 nm; spectral resolution 1.27 nm and 0.265 nm pixel^{-1}) of the Type Ia supernova (SN Ia) 2001el was obtained with the ESO Very Large Telescope Melipal (+FORS1) at five epochs. The spectra a week before maximum and around maximum indicate photospheric expansion velocities of about 10,000 km s^{-1}. Prior to optical maximum, the linear polarization of the continuum was ≈0.2%–0.3% with a constant position angle, showing that SN 2001el has a well-defined axis of symmetry. The polarization was nearly undetectable a week after optical maximum. The spectra are similar to those of the normally bright SN 1994D, with the exception of a strong double-troughed absorption feature seen around 800 nm (FWHM about 22 nm). The 800 nm feature is probably due to the Ca II IR triplet at very high velocities (20,000–26,000 km s^{-1}) involving ∼0.004 $M_\odot$ of calcium and perhaps 0.1 $M_\odot$ total mass. The 800 nm feature is distinct in velocity space from the photospheric Ca II IR triplet and has a significantly higher degree of polarization (≈0.7%) and different polarization angle than the continuum. Taken together, these aspects suggest that this high-velocity calcium is a kinematically distinct feature with the matter distributed in a filament, torus, or array of "blobs" almost edge-on to the line of sight. This feature could thus be an important clue to the binary nature of SNe Ia, perhaps associated with an accretion disk, or to the nature of the thermonuclear burning, perhaps representing a stream of material ballistically ejected from the site of the deflagration to detonation transition. If modeled in terms of an oblate spheroid, the continuum polarization implies a minor to major axis ratio of around 0.9 if seen equator-on; this level of asymmetry would produce an absolute luminosity dispersion of about 0.1 mag when viewed at different viewing angles. If typical for SNe Ia, this would create an rms scatter of several hundredths of a magnitude around the mean brightness–decline relation. We discuss the possible implications of this scatter for the high-precision measurements required to determine the cosmological equation of state.

Subject headings: galaxies: individual (NGC 1448) — supernovae: general — supernovae: individual (SN 2001el) — techniques: polarimetric

On-line material: color figures

1. INTRODUCTION

The last decade has witnessed an explosive growth of high-quality data and models for supernovae with spectacular results that provided new perspectives for the use of Type Ia supernovae (SNe Ia) as cosmological yardsticks and for constraining the physics of supernovae. SNe Ia have provided new estimates for the value of the Hubble constant (H_0) with 10% uncertainty based on a purely empirical procedure (Hamuy et al. 1996; Riess, Press, & Kirshner 1996) and on a comparison of detailed theoretical models with observations (Höflich & Khokhlov 1996; Nugent et al. 1997). More recently, the routine successful detection of supernovae at large redshifts, z (Perlmutter et al. 1997; Riess et al. 1998), provided results that are consistent with a low matter density in the universe and, most intriguing of all, yielded hints for a positive cosmological constant, $\Omega_\Lambda \approx 0.7$, and prompted the quest for the nature of the "dark energy" or cosmological equation of state (Perlmutter, Turner, & White 1999). To pursue these issues with SNe Ia, the required photometric accuracy has to be better than 2%–5% (Weller & Albrecht 2002). This raises systematic effects as the main source of concern (Höflich, Wheeler, & Thielemann 1998). In this context, it is important to understand observationally whether or not SNe Ia are spherically symmetric since any deviations from sphericity could potentially affect the accuracy of distance estimates.

Aside from the new focus on SNe Ia as cosmological tools, there are long-standing problems associated with determining the progenitor evolution and the physical processes involved in the explosion by thermonuclear combustion. It is nearly universally assumed that SNe Ia result from some form of binary evolution, but no direct observational evidence for this conjecture has ever been presented. There is also general agreement that SNe Ia result from some process involving the combustion of a degenerate white dwarf (WD; Hoyle & Fowler 1960). Within this general picture, three classes of models have been considered: (1) an explosion of a carbon/oxygen (CO) WD, with mass close to the Chandrasekhar limit, that accretes mass through Roche lobe overflow from an evolved companion star (Whelan & Iben 1973); (2) an explosion of a rotating configuration formed from the merging of two low-mass WDs, caused by

[1] Based on observations collected at the European Southern Observatory, Chile (ESO Programme 68.D-0571(A).

[2] Lawrence Berkeley National Laboratory 50-232, 1 Cyclotron Road, Berkeley, CA 94720.

[3] European Southern Observatory, Karl-Schwarzschild-Strasse 2, D-85748 Garching, Germany.

[4] Department of Astronomy and McDonald Observatory, University of Texas at Austin, Austin, TX 78712.

[5] Laboratory for Computational Physics and Fluid Dynamics, Naval Research Laboratory, Washington, DC 20375; ajk@lcp.nrl.navy.mil.

[6] Stockholm Observatory, AlbaNova, Department of Astronomy SE-106 91, Stockholm, Sweden.

the loss of angular momentum through gravitational radiation (Webbink 1984; Iben & Tutukov 1984; Paczyński 1985); and (3) explosion of a low-mass CO WD triggered by the detonation of a helium layer (Weaver, Axelrod, & Woosley 1980; Wallace & Woosley 1981; Nomoto 1982; Woosley & Weaver 1986). Only the first two models appear to be viable for observed SNe Ia (Höflich & Khokhlov 1996; Nugent et al. 1997). Although not favored for most SNe Ia, the merging of two WDs may contribute to the SN Ia population, particularly, perhaps, to subluminous events (Howell et al. 2001). All three scenarios might leave some trace in polarization data.

There are at least three ways in which the fact that SNe Ia evolve and explode in binary systems could impart a dominant axis to the explosion that could be reflected in the polarization. Perhaps the most general is that the WD could be rotating. Rotation could affect the shape of the WD, or it could affect the propagation of the thermonuclear burning (see below) and hence the distribution of either the elements produced or the density or both (Howell et al. 2001). Another generic asymmetric feature is an accretion disk. Accretion disks resulting from mass transfer are not expected to be very massive, and hence it is difficult to see how the swept up disk matter could directly affect the asymmetry. The exception might be if the disk comes from the disruption of a binary WD companion, in which case the remnant disk at the time of the explosion could be thick and dense. A third asymmetry generic to binary evolution models for SNe Ia is a binary companion. In two of the scenarios, the $M_{\rm Ch}$ models and the helium detonators, the binary companion should still exist. The collision of the ejecta with this companion must induce some level of asymmetry in the ejecta (Livne, Tuchman, & Wheeler 1992; Marietta, Burrows, & Fryxell 2000).

Other asymmetries, especially departures from a dominant axis of symmetry, could be intrinsic to the explosion process. The departures from the dominant axis could come from lumps of ^{56}Ni that produce irregularities in the excitation. These, in turn, would be clues to the nature of the thermonuclear burning that drives the explosion. Within the class of $M_{\rm Ch}$ models, it is believed that the explosion is triggered by compressional heating near the WD center and that the burning front starts as a subsonic deflagration. The time evolution of the burning front is still an open question. The issue is whether the deflagration front burns through the entire WD (Nomoto, Thielemann, & Yokoi 1984) or makes a transition into a supersonic detonation mode, as suggested in the delayed detonation (DD) model (Khokhlov 1991; Yamaoka et al. 1992). DD models have been found to reproduce the optical and infrared light curves and spectra of "typical" SNe Ia reasonably well (Höflich 1995b; Höflich & Khokhlov 1996; Nugent et al. 1997; Wheeler et al. 1998; Lentz et al. 2001). The propagation of a detonation front is well understood (Gamezo et al. 1999; Sharpe 2001), but the description of the deflagration front and the deflagration to detonation transition pose problems.

Significant progress has been made toward a better understanding of the physics of thermonuclear flames. The front has been found to be Rayleigh-Taylor (RT) unstable, increasing the effective speed of the burning front (Nomoto, Sugimoto, & Neo 1976) and also, perhaps, imposing density irregularities (plumes) on the structure that could be reflected in the polarimetry. Starting from static WDs, hydrodynamic calculations of the deflagration fronts have been performed in two dimensions (Reinecke, Hillebrandt, & Niemeyer 1999) and three dimensions (Livne 1993; Khokhlov 1995; Khokhlov 2002). RT instabilities govern the morphology of the burning front, and the effective burning speed is very sensitive to the energy release by the fuel and therefore to the local C/O ratio (Khokhlov 2002). Therefore, the actual flame propagation will depend on the detailed chemical structure of the progenitor. Three-dimensional models (Khokhlov 2002) suggest that plumes of burned matter are frozen out in the expansion. These plumes, rich in ^{56}Ni, could be the source of dispersion around any dominant polarization axis. On the other hand, optical and IR data on the subluminous but significantly polarized SN 1999by (Howell et al. 2001) seem to be at odds with these models of the deflagration phase that predict significant mixing of the inner layers of the WD prior to detonation. Whether this conflict exists for normally bright SNe Ia remains to be seen. The transition to detonation is thought to occur earlier in normally bright events, giving less time for the RT structure to develop. This might allow clumps of ^{56}Ni to develop that could drive the dispersion in polarization vectors without causing intolerably large distortions of the flux spectrum.

Preconditioning of the WD may affect the nature of both normal and subluminous SNe Ia. Such preconditioning may involve the main-sequence mass and metallicity of the progenitor WD (Domínguez, Höflich, & Straniero 2001; Höflich et al. 1998; Iwamoto et al. 1999), the accretion history (Langer et al. 2000), large-scale velocity fields such as turbulence prior to the runaway (Höflich & Stein 2002), or rotation (Howell et al. 2001).

A picture of the geometrical structure of different chemical constituents of different varieties of SN Ia can thus be crucial for constraining the physical models of the progenitor evolution and explosion. During the first few weeks after the explosion, the photosphere recedes rapidly from the outermost stellar surface to deep inside the metal-rich central regions where the chemical composition is heavily affected by the explosion. Polarization is a powerful tool to probe the structure of the rapidly expanding matter and to provide detailed information about the geometrical structure of the ejecta that is important in understanding supernova explosions and their subsequent evolution to supernova remnants. Polarimetry can also be used to probe the preexplosion environment and the properties of the ISM along the line of sight.

Wang et al. (1996) and Wang, Wheeler, & Höflich (1997) reported polarimetry data obtained at McDonald Observatory. They studied supernova polarimetry published before 1996 and found that Type Ia supernovae are normally not polarized and on average show much lower polarization than core-collapse supernovae (Type II, Ib/c). The degree of polarization of most SNe Ia observed in Wang et al. (1996, 1997) is unlikely to be higher than 0.2%–0.3% at the observed epochs. The data also indicate a higher degree of polarization for the bare-core or low-mass events such as Type IIb and Ib/c supernovae than for more massive ejecta (Wang et al. 2001a). The degree of polarization is a function of time after explosion. For core-collapse events, the degree of polarization is higher past optical maximum than before optical maximum (Wang et al. 2001a; Leonard et al. 2000, 2001; Leonard & Filippenko 2001). These conclusions were based on only a few events, and not all types of supernovae were covered.

Spectropolarimetric observations of SNe Ia and interpretation of the data are both very difficult, as emphasized in Wang et al. (1997). Because of the large number of overlapping Fe II lines in an SN Ia atmosphere, polarization features of SNe Ia are usually harder to detect and interpret than those of SNe II. For SNe II, lines of Hα and Na I/He I 5876 Å normally stand out and a geometrical picture can be built based on these lines. Further analysis of other chemical components can be constructed following the structure deduced from the stronger lines. Wang et al. (1997) argue that despite the rather noisy appearance of the spectropolarimetry of SN 1996X, polarization of degree around 0.25% may have been detected by comparing the observed data with model calculations of SN Ia polarization spectra. The only SN Ia published so far that showed a clear polarization signal of about 0.7% is the subluminous event SN 1999by, which at optical maximum had a chemical structure very different than that of normal SNe Ia (Howell et al. 2001). It thus remains an extremely interesting question to investigate the polarization of spectroscopically normal SNe Ia and other subclasses of SNe Ia.

In this paper, we present in § 2 observations and data reduction of SN 2001el. We discuss the spectroscopic and spectropolarimetric evolution in § 3 and § 4, respectively. The structure of the SN 2001el ejecta is studied in § 5. In § 6, we give a discussion and conclusions with emphasis on implications for progenitor models of SNe Ia and the effect of asymmetry on SN Ia luminosity. Detailed discussions of the structure of the ejecta with the focus on the Ca II features are given in a separate paper by Kasen et al. (2003).

2. OBSERVATIONS AND DATA REDUCTION OF SN 2001el IN NGC 1448

The bright SN Ia event SN 2001el provided a rare chance to study the structure of a thermonuclear explosion. An image taken by the Very Large Telescope (VLT) with FORS1 in imaging mode is shown in Figure 1. The SN was discovered visually on September 17.064 UT at a magnitude of about 14.5 (Monard 2001). The host, NGC 1448, is a spiral galaxy nearly edge-on with major axis at a position angle of around 45°. Galactic reddening on the line of sight to NGC 1448 is $E(B-V) = 0.014$ mag (Schlegel, Finkbeiner, & Davis 1998). The supernova is located at R.A. = $3^{h}44^{m}30^{s}.60$, decl. = $-44°38'23''.4$ (equinox J2000.0), which is 14″ west and 20″ north of the nucleus of NGC 1448. The line of sight does not intersect the core or disk of NGC 1448, so extinction within the host galaxy should be small. The SN was not detected down to 14.6 on August 25.96 and was seen rising in brightness the night after discovery (Monard 2001). The peak magnitude was $V = 12.7$ mag on about October 1 (N. Suntzeff 2001, private communication). It was classified as an SN Ia well before maximum based on spectroscopic data taken using the ESO-VLT Kueyen with the UVES, an echelle spectrograph, by Sollerman, Leibundgut, & Lundqvist (2001), who also noticed that the characteristic Si II absorption at 612 nm appeared to be flat bottomed. The ESO UVES data also show interstellar absorption lines of Ca II H and K, and lines of Na I D with equivalent widths of 0.037 and 0.031 nm, respectively, at the redshift (1162 km s^{-1}) of NGC 1448. The first set of spectropolarimetry data was obtained on September 26 UT using the ESO-VLT Melipal with FORS1 (Wang et al. 2001b), for which we reported spectral features and the positive detection of polarization at about 0.7%—comparable to what is normally observed for Type II supernovae.

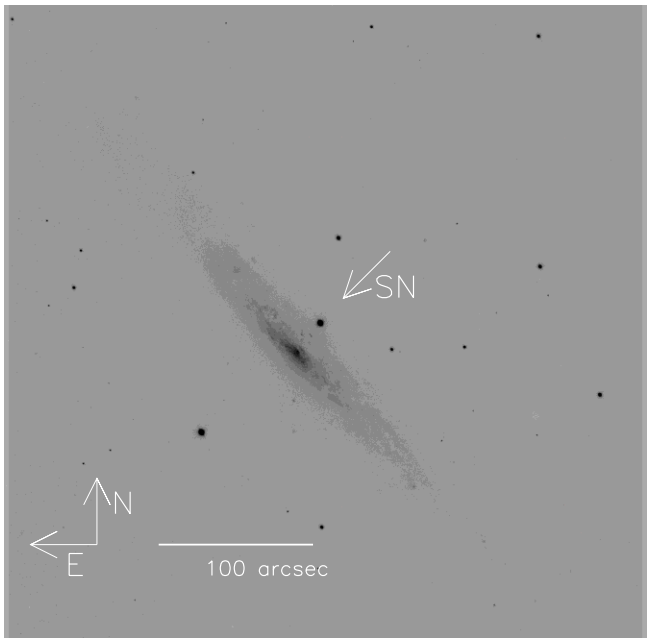

FIG. 1.—Field of SN 2001el and the host galaxy NGC 1448. The SN is marked by the arrow.

We subsequently decided to obtain spectropolarimetry of SN 2001el in great detail for two purposes. First, we want to obtain data of superb quality so that we can establish firmly the characteristics of a definitely polarized SN Ia. This knowledge can then be used to assess the degree to which we can trust other data sets—both those observed from the VLT and those obtained at smaller telescopes. Second, SN 2001el, for which the maximum luminosity was brighter than 13 mag, provided a rare opportunity to study in great detail the nature of SNe Ia. We planned the observations so that the evolution from before optical maximum to close to the nebular phase was well covered. We also tried to guess the location of the photosphere while planning the observations so that important epochs where the photosphere crossed a chemical layer could be probed.

All of these observations were obtained in service mode through our Target-of-Opportunity program at the VLT Melipal with FORS1. FORS1 employs a TK2048EB4-1 2048 × 2048 backside-illuminated thinned CCD. The cooling of the CCD is performed by a standard ESO bath cryostat. This system uses a FIERA controller for CCD readout. The grism GRIS-300V (ESO number 10) was used for all observations. The order separation filter GG 435+31 (4) was used in some observations to study the Ca II IR triplet but was also taken out to observe spectral features in the blue end. The supernova was always observed in four subsequent separate exposures with the position angle of the Wollaston prism at 0°.0, 45°.0, 22°.5, and 67°.5. The $\lambda/2$ retarder plates are of the "superachromatic" type, and the position angles can be set with an accuracy of 0°.1. The chromatic zero angles were set by the data provided in the VLT FORS1 user manual (Böhnhardt & Szeifert 2002). The spatial scale is about 0″.20 pixel^{-1}. The spectral resolution for these observations is around 12.7 Å as measured from the spectral calibration lamps, with each pixel corresponding to

TABLE 1
LOG OF OBSERVATIONS OF SN 2001el

Date (2001)	Exposure (s)	Wavelength (nm)	Air Mass	Grism	Filter
Sep 26.284.....	4 × 60	418.1–863.5	1.11	GRIS-300V	GG 435
Sep 26.297.....	4 × 480	418.1–863.5	1.10	GRIS-300V	GG 435
Oct 01.205.....	4 × 500	418.1–863.5	1.30	GRIS-300V	GG 435
Oct 09.240.....	60.0	333.0–863.4	1.12	GRIS-300V	...
Oct 09.243.....	4 × 240.0	333.0–863.4	1.11	GRIS-300V	...
Oct 09.261.....	4 × 400.0	418.1–8635	1.10	GRIS-300V	GG 435
Oct 18.161.....	4 × 500	418.1–8635	1.29	GRIS-300V	GG 435
Oct 18.191.....	4 × 500	333.0–8634	1.18	GRIS-300V	...
Oct 09.101.....	4 × 1200	333.0–863.4	1.29	GRIS-300V	...

about 2.6 Å in wavelength scale. A 1″.0 wide slit is used for all these observations.

A log of observations is presented in Table 1. In addition to the observations listed in Table 1, we have also obtained images for bias correction, wavelength calibration, and flat-fielding for each observing run. The wavelength calibration and flat-fielding images are all obtained with the wave plate rotated to the same position angles used for the supernova observations, i.e., 0°.0, 45°.0, 22°.5, and 67°.5. The flat-field images of each run are combined to form the final flat-field correction image that is applied to each data set. Standard data reduction procedures including bias correction, flat-fielding, background subtraction, spectrum extraction, wavelength calibration, and flux calibration were performed using the IRAF package (Tody 1993). The polarized spectra were reduced using our own software. The per pixel photon statistical errors of the Q and U vectors of the VLT data were typically below 0.1%. Because polarimetry involves the difference of the ordinary and extraordinary light, the per pixel errors are normally exaggerated and are artificial because each resolution element contains more than one pixel. It is always useful to rebin the data into bin sizes comparable to the spectral resolution to reduce the artificial per pixel errors and error correlations. In this paper, all Stokes parameters were rebinned to a 15 Å interval. The binning was done by calculating the average polarization within a bin weighted by the number of detected photons within each pixel (Wang et al. 1997). The 15 Å binning was chosen so that it is slightly larger than the spectral resolution of the data (12.7 Å) to eliminate sampling errors of the resolution element. The rebinning is equivalent to calculating the degree of polarization of all photons integrated in each bin; when the bin size is larger than the resolution element, the errors of the Stokes parameters in each wavelength bin are uncorrelated. Typical photon statistical errors in the Q and U vector after binning to the 15 Å interval are around 0.02% for all of these observations and are not a major source of error in the discussion of these data. During the commissioning of FORS1 in 1998/1999 the systematic instrumental polarization of FORS1 was found to be less than 0.1% (T. Szeifert 1999, private communication). Errors during data reduction are expected to be small as well (<0.02%) because the data are reduced in double precision.

3. SPECTROSCOPIC PROPERTIES OF SN 2001el

Figure 2 shows the spectral evolution of SN 2001el. The date of B maximum of SN 2001el was found by Krisciunas et al. (2003) to be September 31, from which we found that our spectra were taken at −4, +1, +10, +19, and +41 days from B maximum, respectively. SN 2001el would be a spectroscopically normal supernova had the wavelengths beyond 750 nm not been observed in the premaximum phase. The match of spectral features to SN 1994D is extremely good except for the vicinity of the Ca II IR triplet. The Ca II IR triplet is clearly detected in all our spectra of SN 2001el with a strength that grows in time at a velocity around −10,000 km s^{-1}, close to the velocities given by other photospheric lines such as Si II 635.5 nm. The feature that distinguishes SN 2001el is a distinctively strong absorption at around 800 nm. As argued below, we interpret this as

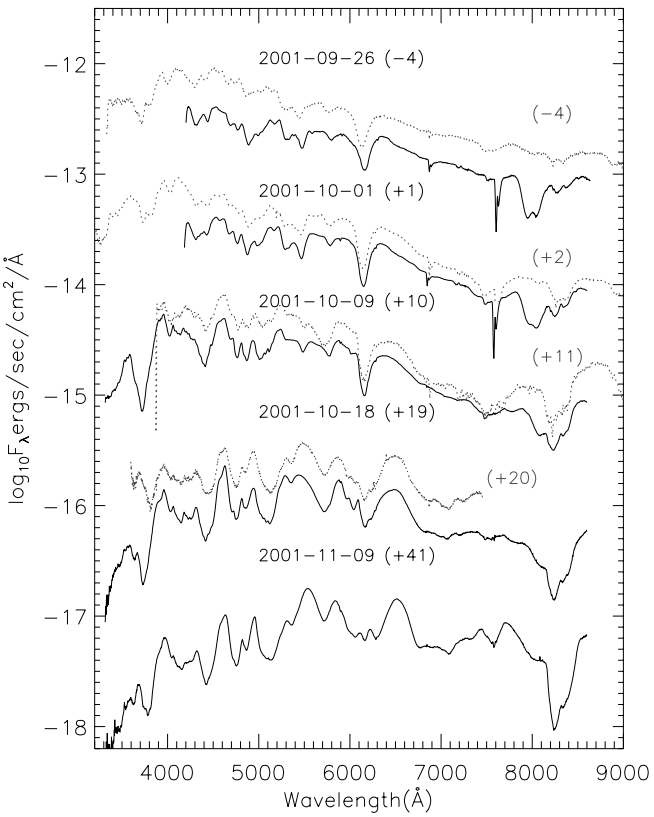

FIG. 2.—Spectral evolution of SN 2001el. The spectra are similar to those of normal SNe Ia except for the strong absorption line at around 800 nm. Spectra of SN 1994D (*dotted lines*) are also shown for comparison. The phases of the SN 1994D data are day −4, +2, +11, and +20 from top to bottom. The absorption line at 800 nm is seen in premaximum spectra of SN 1994D as well but is much weaker than that of SN 2001el. This line could be due to a high-velocity component of the Ca II IR triplet. [*See the electronic edition of the Journal for a color version of this figure.*]

a kinematically and geometrically separate filament or shell of calcium-rich material.

SN 1994D and other SNe Ia have shown weak features corresponding to the Ca II IR triplet at high velocities with a double-humped absorption minimum (Hatano et al. 1999). Models of SN 1994D showed that the Ca II IR triplet can form a feature with a two-component absorption minimum (Höflich 1995b; Höflich et al. 1998, their Fig. 9) but that the double-minimum structure is primarily dictated by the density and temperature through the ionization in such a way that the feature should recede in velocity as the ejecta expand. Although the 800 nm feature fades with the approach to maximum light, it always remains distinct from the photospheric Ca II IR triplet feature as the latter gains in strength. The 800 nm feature does not seem to evolve substantially in velocity space. In addition, the postmaximum photospheric component of the Ca II IR triplet in SN 2001el has a sharp blue edge at a velocity of around −12,500 km s^{-1} (see the last two spectra at +16 and +38 days in Fig. 2). This implies that there is a sharp density drop of Ca at that velocity. On the other hand, the premaximum line profiles of the 800 nm feature show rather sharp edges that, if identified with Ca II, correspond to a velocity of about 15,000–20,000 km s^{-1} on the red side and about 26,000 km s^{-1} on the blue side (see the top spectrum in Fig. 2). The polarization data accentuate this delineation in velocity space, as shown in the top panels corresponding to the data on September 26 in Figure 3. In any case, the red edge of the

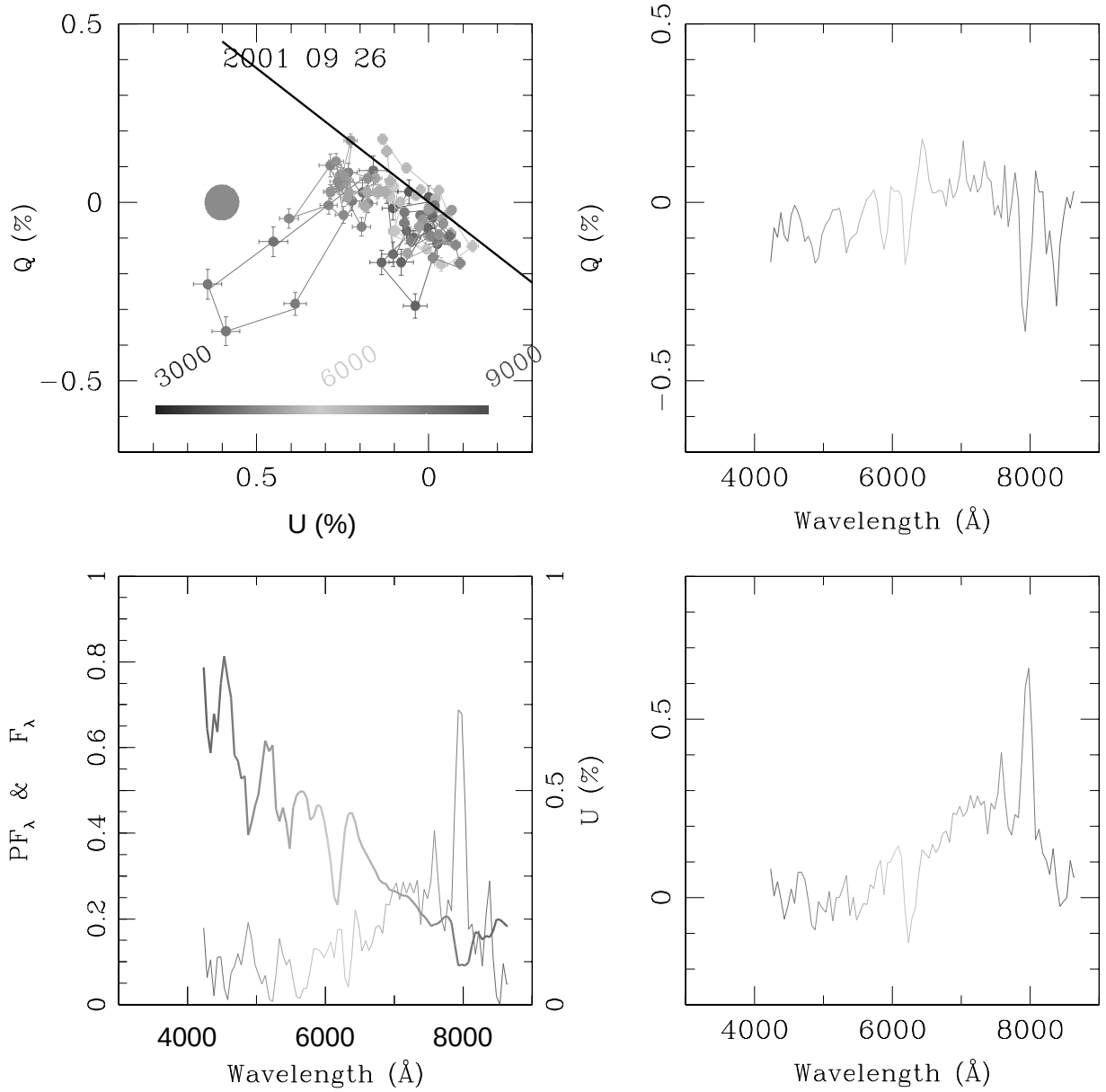

FIG. 3.—Spectropolarimetry of SN 2001el on 2001 September 26, 7 days before maximum. The Stokes parameters are rebinned into 15 Å bins. An interstellar polarization component is subtracted from the observed Stokes parameters so that the data points represent intrinsic polarization due to the supernova. The assumed interstellar polarization is shown as a filled circle in the *Q*-*U* plot (*upper left*). Without subtraction of the interstellar component, the origin of the coordinates would be centered at this filled circle. The straight line illustrates the dominant axis shifted to the origin of the *Q*-*U* plot. The *Q* (*upper right*) and *U* (*lower right*) spectra show conspicuously polarized spectral features. The degree of polarization is shown as the thin line in the lower left panel with the flux spectrum (*lower left panel*, *thick line*) overplotted to show the correlations of the degree of polarization and the spectral features. The wavelength color code is presented at the bottom of the upper left panel. [*See the electronic edition of the Journal for a color version of this figure.*]

high-velocity feature at the top of Figure 2 does not overlap with the blue edge of the low-velocity Ca II feature at the bottom of Figure 2. If both of these absorptions are due to the Ca II IR triplet, this implies that the high-velocity filament or shell also has rather well defined geometrical boundaries.

The polarization data suggest that the lowest velocity matter in this high-velocity feature might be at about 17,000 km s^{-1} if the feature is Ca II. The polarization shows that this feature also has a different geometrical orientation than the geometry that defines the dominant axis of the photosphere. Taken together, the velocity separation, the large amplitude of the polarization, and the different polarization angle all imply that this feature is a kinematically and geometrically separate high-velocity component that is enriched in calcium.

It is difficult to see whether something like this separate high-velocity feature exists in other SNe Ia. The kinematic boundaries of the high-velocity calcium are impossible to discern in the data of SN 1994D, since the feature is so much weaker. A search of published SN Ia spectra shows that most of the SNe Ia with premaximum spectra covering the 800 nm area reveal weak spectral features similar to that of SN 1994D. As for SN 1994D, however, it is difficult to discern whether this high-velocity component is geometrically "detached" from the photospheric structure when the line is weak. In addition, the presence of Fe II absorption at about 800 nm can obscure the nature of this feature. The current SN Ia data base does seem to suggest that the very strong feature, definitely displaced from the photospheric Ca II IR triplet, is rather special to SN 2001el. We address the possible physical origin of this feature in § 5.

4. SPECTROPOLARIMETRY PROPERTIES OF SN 2001el

Wang et al. (2001a) outlined a method to decompose the observed polarimetry into two components. On the *Q-U*

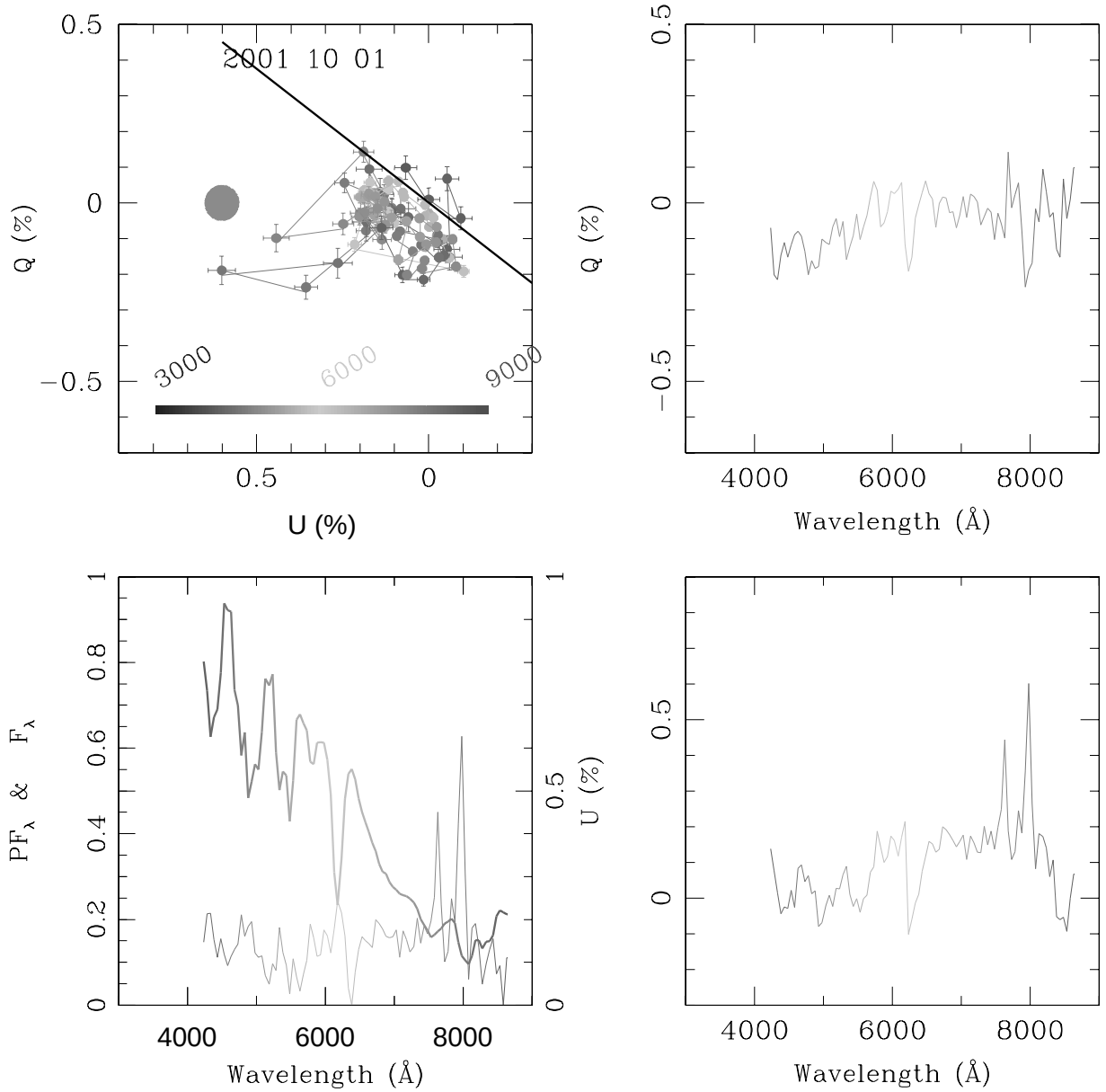

FIG. 4.—Same as Fig. 3 but for data taken on October 1, 2 days before maximum. [*See the electronic edition of the Journal for a color version of this figure.*]

plot, the two components correspond to the polarized vectors projected onto the so-called dominant axis and the axis perpendicular to the dominant axis. The dominant axis can be defined from the aspherical distribution of the data points on the *Q*-*U* plane. The dominant axis is derived by a linear fit to the data points weighted by the observational errors in the *Q*-*U* plane. The spectropolarimetry projected to the dominant axis represents global geometric deviations from spherical symmetry, whereas the vector perpendicular to the dominant axis represents deviations from the dominant axis. The same method is applied in this study as well.

We show in Figures 3–7 the observed data points in the *Q*-*U* plane. Each point represents a data pair of the *Q*-*U* vector at a different wavelength. The wavelengths of the data points in important intervals are encoded in color. The data show remarkable evolution during the five epochs of observation. The polarization also shows spectral features that can be identified with features in the flux spectra. This firmly establishes that SN 2001el is intrinsically polarized, at least at certain epochs after explosion.

SN 2001el exhibits some remarkable features that are unlike those of previously observed SNe II and the subluminous SN Ia 1999by (Wang et al. 1996; Wang et al. 1997, 2001a; Leonard & Filippenko 2001; Leonard et al. 2001; Howell et al. 2001). On the *Q*-*U* plot, SN 1998S and SN 1999by showed well-defined linear features (Wang et al. 2001a; Howell et al. 2001). This is indicative of a relatively well defined symmetry axis. The SN 2001el data, however, show large scatter around the dominant axis. In particular, a sharp increase of the degree of polarization is seen in the Ca II IR triplet in the September 26 and October 1 data. Other strong polarized spectral features are also observed

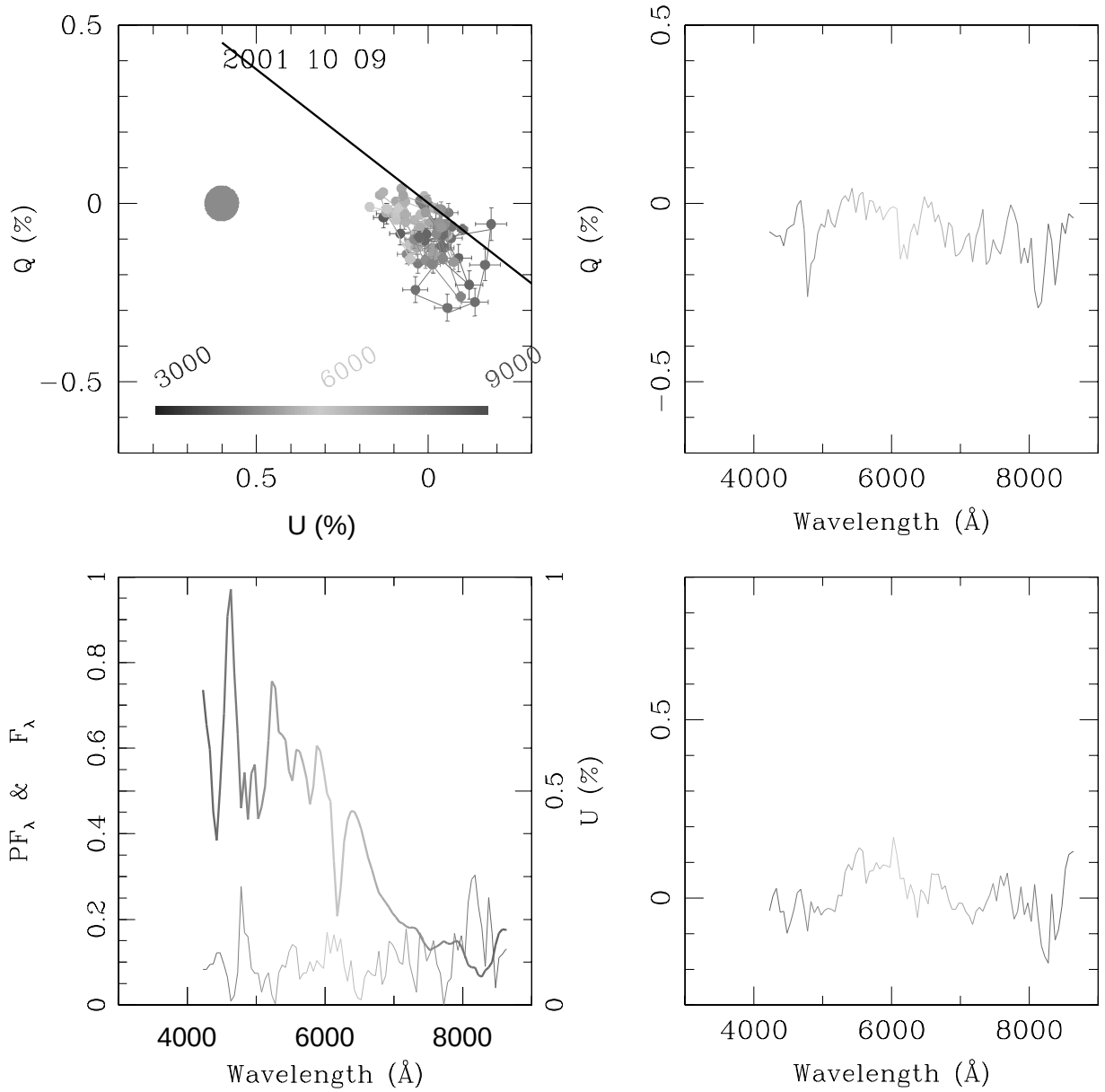

FIG. 5.—Same as Fig. 3 but for data taken on October 9, 7 days after maximum. [*See the electronic edition of the Journal for a color version of this figure.*]

during September 26 and October 1. The polarized features become much weaker in the data taken on October 18 and afterward.

4.1. *Interstellar Polarization*

To derive the intrinsic polarization due to the supernova atmosphere, we first need to deduce the component due to interstellar dust. A simple approach is to assume that the resonance-scattered photons are unpolarized (Trammell, Hines, & Wheeler 1993). This method attempts to distinguish continuum and scattered photons and use that separation to derive interstellar extinction (Jeffrey 1991; Trammell et al. 1993; Höflich et al. 1996; Wang et al. 1996; Tran et al. 1997; Leonard & Filippenko 2001). This technique implicitly assumes a unique intrinsic polarimetry axis, and the derived interstellar polarization should fall on the dominant axis. The interstellar polarization derived from this method, however, is normally inconsistent with the initial assumptions. In the case of SN 1993J, it is also clear from the data in the Q-U plane that there are significant deviations from the dominant axis (Wang et al. 2001a). Another method is outlined in Wang et al. (2001a) that relaxes the constraints on the polarization properties of emission lines and assumes only that at each specific epoch, the polarization produced by the supernova ejecta has a single polarization position angle independent of wavelength. This method would set the interstellar polarization at one of the two ends of the dominant axis. This method, again, is perhaps a useful method only for those data with a well-defined dominant axis.

Neither of the above two methods is applicable for the SN Ia data discussed in this paper. The time evolution of the polarization data in fact shows that the degree of polarization decreases significantly after maximum light. The data taken on 2001 November 9, in particular, show flat Q and U

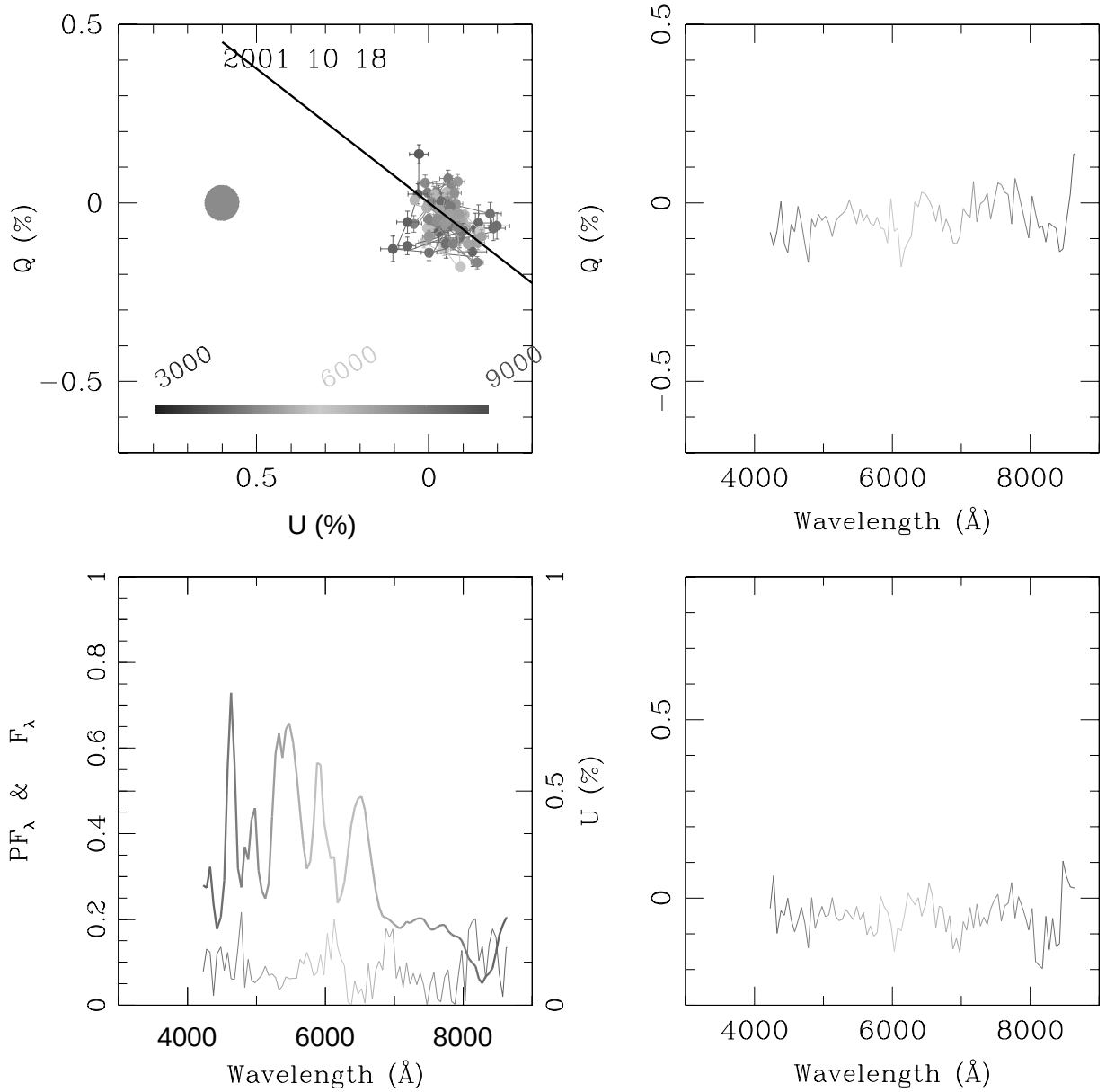

FIG. 6.—Same as Fig. 3 but for data taken on October 18, 16 days after maximum. [*See the electronic edition of the Journal for a color version of this figure.*]

spectra with little evidence of deviations across most of the strong lines. At this phase, the supernova has entered the nebular phase, and there are substantial reasons to believe that the ejecta have become optically thin to electron scattering. Intrinsic polarization due to the supernova ejecta should be small at this phase. The right panels of Figure 7 show that there are perhaps still detectable polarized features at the P Cygni absorption dip of the Ca II IR triplet, but the degree is significantly smaller than for earlier epochs. In wavelength regions excluding the Ca II IR triplet feature, the fluctuations of the polarization are about 0.1%—consistent with earlier observations on other post-maximum SNe Ia. If we assume that at this epoch in the wavelength range 430–500 nm the supernova is intrinsically unpolarized, we find the interstellar polarization to be at $Q = 0.01 \pm 0.05$ and $U = 0.60 \pm 0.05$. We will adopt this as the best estimate of the interstellar polarization.

The Galactic extinction is $E(B-V) = 0.014$ (Schlegel et al. 1998), which would produce a maximum degree of polarization of 0.13% (Serkowski, Mathewson, & Ford 1975)—too small to account for the 0.6% interstellar polarization. According to Serkowski et al. (1975), the observed interstellar polarization implies that the total extinction to the supernova is larger than $E(B-V) = 0.067$, with the extinction by the host galaxy being larger than 0.053.

The wavelength dependence of the interstellar polarization gives reasonable estimates of the properties of the dust particles on the line of sight to the supernova. A fit to the empirical formula (Serkowski et al. 1975; Wilking, Lebofsky, & Rieke 1982) with the September 9 data binned to 60 nm is shown in Figure 8. The fit shows that the wavelength at which the polarization reaches maximum is $\lambda_{max} = 514 \pm 10$ nm. For comparison, the Galactic value of λ_{max} is around 550 nm. The fit implies that the dust that is responsi-

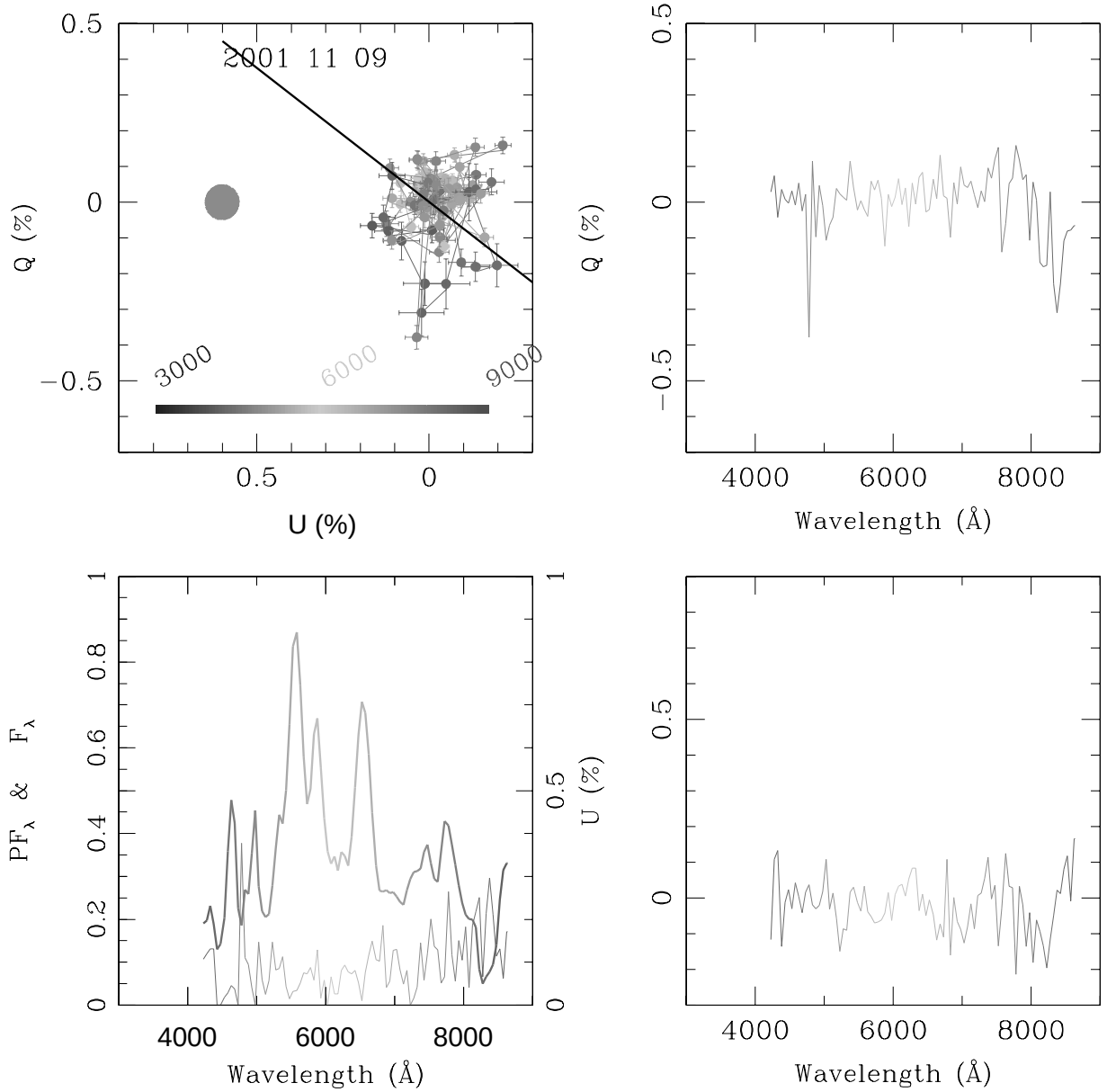

FIG. 7.—Same as Fig. 3 but for data taken on November 11, 38 days after maximum, with the data rebinned to 50 Å. [*See the electronic edition of the Journal for a color version of this figure.*]

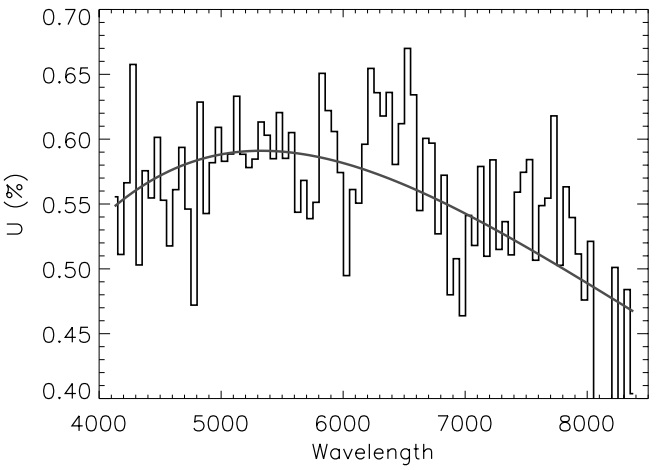

FIG. 8.—Fit to the interstellar dust polarization using the empirical Serkowski law $p_\lambda/p_{\max} = \exp[-K \ln^2(\lambda_{\max}/\lambda)]$ (Wilking et al. 1982; Serkowski et al. 1975). The data are from September 9 observations. [*See the electronic edition of the Journal for a color version of this figure.*]

ble for the interstellar polarization is similar to that of the Galaxy. Adopting the relation $R_v = (5.6 \pm 0.3) \times 10^{-4} \lambda_{\max}$ (Serkowski et al. 1975; Larson, Whittet, & Hough 1996; Whittet et al. 2001), we found that $R_v = 2.88 \pm 0.15$.

The above analysis yields a polarization position angle of 45° for the interstellar polarization. This implies that the magnetic field is parallel to the disk of the host galaxy (cf. Fig. 1).

4.2. *Decomposition of the Polarization*

With the above choice of interstellar polarization, we can now decompose the observed polarization into the two components as described in the introduction to § 4. The new coordinates are given by rotating the original coordinate systems counterclockwise so that the Q axis overlaps the dominant axis in the new coordinate system. The dominant axis is determined to be at position angle $\alpha = -26\overset{\circ}{.}57$ through a linear fit to the data points on the Q-U plot of September 26. We have rotated the Q-U coordinate system by $26\overset{\circ}{.}57$ clockwise so that the dominant axis points toward the center of the data cluster on the Q-U plot. The components parallel and perpendicular to the dominant axis are given by

$$P_d = (Q - Q_{\rm ISP}) \cos 2\alpha + (U - U_{\rm ISP}) \sin 2\alpha \qquad (1)$$

and

$$P_o = -(Q - Q_{\rm ISP}) \sin 2\alpha + (U - U_{\rm ISP}) \cos 2\alpha \,, \qquad (2)$$

where P_d and P_o are the polarization components parallel to the dominant axis and orthogonal to that axis, respectively, and $Q_{\rm ISP}$ and $U_{\rm ISP}$ are the Stokes parameters of the interstellar polarization.

To understand the physical meaning of the new coordinate system, it is useful to start from the simple spheroid models described in Höflich et al. (1996) and Wang, Wheeler, & Höflich (1997). In those models, the polarization is produced by electron scattering through an aspherical atmosphere, and the spectropolarimetric lines are formed because of line scattering. Such a geometry would produce a single line on the Q-U plot, with the wavelength region that suffered the most line scattering being most depolarized and hence the closest to the origin. Such an ideal system apparently does not apply to SN 2001el, where, as can be clearly seen, the Q-U vectors show significant scatter around the dominant axis. The spheroid model can be modified to account for the scatter. For example, chemical clumps and filaments are reasonable sources for deviations from the single-axis geometry.

Under the modified spheroid scenario, the dominant axis most likely measures the global departure of the photosphere from spherical symmetry. In the case of an axially symmetric spheroid, P_o measures the deviations and fluctuations from axial symmetry.

P_d and P_o are plotted in Figure 9, where it can be seen that the P_o components are flat for these observations except for the spectral features due to a few strong lines. Most of the continuum polarization is recorded in P_d. The wavelength at which the degree of polarization reaches maximum was around 740 nm on September 26 and moved to about 670 nm on October 1 and 550 nm on October 9. The P_d distribution became practically flat on October 18 and November 9. The fact that the October 18 and November 9 polarization spectra are flat again supports our choice of interstellar polarization. The polarized flux of the dominant component P_d peaked at 650, 610, and 550 nm on September 26, October 1, and October 9, respectively, and became flat on October 18 and November 9. For the spheroid model of Höflich et al. (1996) and Wang, Wheeler, & Höflich (1997), the blueward evolution of the peak of the polarized flux indicates that the last scattering region was moving toward zones with increasing electron temperature. Polarized spectral features are unambiguously detected around Si II 635.5 nm and the Ca II IR triplet, especially in the first two peaks.

4.3. *Polarization of the* Si II 635.5 nm *Line*

The evolution of the Si II 635.5 nm line is shown in Figure 10. On September 26 and October 1, before optical maximum, the Si II 635.5 nm line is clearly polarized. On the plot for September 26, P_d shows a peak in the velocity range from $-10{,}000$ to 0 km s^{-1}, with a sharp drop at the $-10{,}000$ km s^{-1} edge. The P_o component is practically flat but with a broad weak dip from around $-20{,}000$ to $+10{,}000$ km s^{-1}. On the Q-U plot, the data points of the Si II line form an ellipse elongated along the dominant axis. Similar polarization behavior is seen in Figure 10*b*. The degree of polarization decreased to less than 0.2% on data taken on October 9 and afterward. Note the displacement of the matter moving at $+20{,}000$ km s^{-1} from that at $-20{,}000$ km s^{-1} and the suggestion of a "loop" in the Q-U plane for the matter from 0 to $-10{,}000$ km s^{-1} in Figure 10*a*. In Figure 10*b* the highest velocity components have merged in the Q-U plane, but the suggestion of a "loop" for the 0 to $-10{,}000$ km s^{-1} component remains.

The feature centered in the range $-25{,}000$ to $-20{,}000$ km s^{-1} is especially interesting. It shows peak-to-valley polarization variations of 0.3% and 0.2% on September 26 and October 1, respectively. This feature could be reasonably attributed to a neighboring line, but it is also consistent with being the silicon counterpart of the high-velocity feature observed most clearly in the Ca II IR triplet.

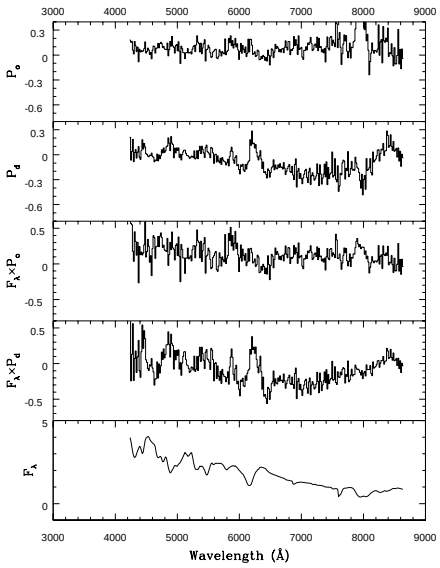

FIG. 9*a*

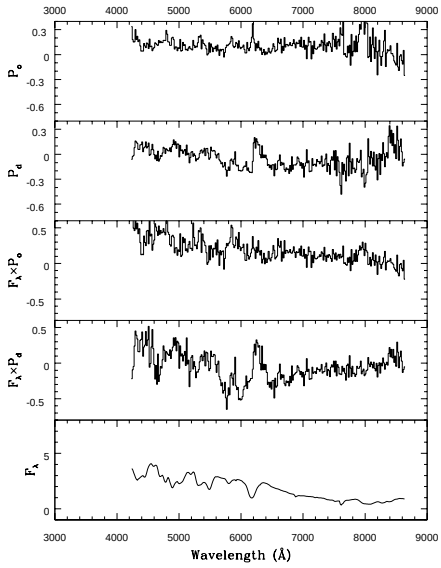

FIG. 9*b*

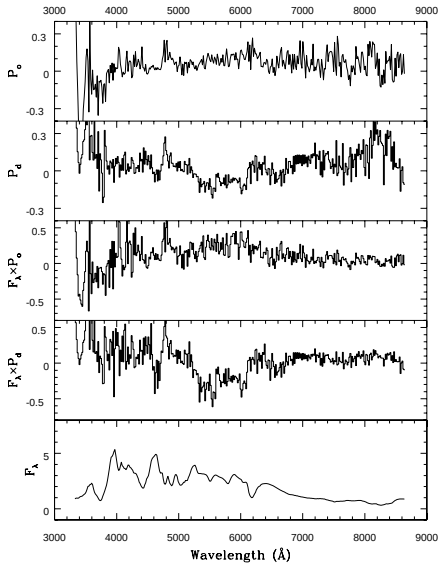

FIG. 9*c*

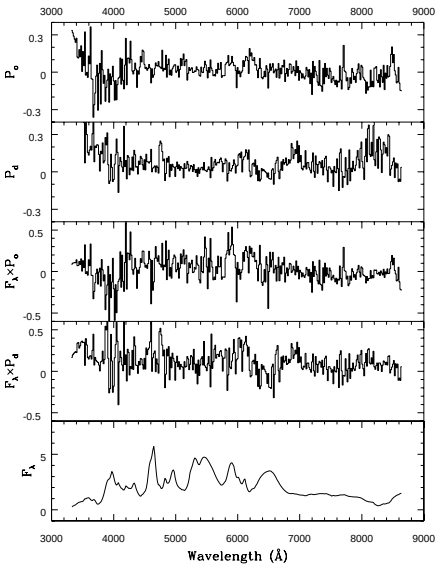

FIG. 9*d*

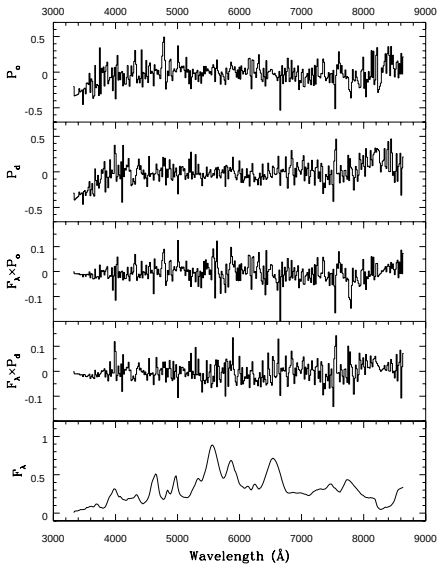

FIG. 9*e*

FIG. 9.—Flux, polarized flux (FP_d and FP_o), P_d, and P_o of SN 2001el on September 26 (*a*), October 1 (*b*), October 9 (*c*), October 18 (*d*), and November 11 (*e*). The flux is in units of 1×10^{-14} ergs cm^{-2} Å^{-1} s^{-1}. The polarized fluxes are in units of 1×10^{-16} ergs cm^{-2} Å^{-1} s^{-1}.

4.4. *Polarization of the* Ca II *IR Triplet*

The strongest polarization is observed for the high-velocity Ca II IR triplet, as shown in Figure 11. The polarization around 800 nm reached 0.7% on September 29 and October 1 while the high-velocity component in the flux spectrum was still strong. The polarization decreased in strength rapidly with the redward evolution of the high-velocity component in the total flux spectrum. The polarization data suggest that the lowest velocity matter in this high-velocity feature might be at about 17,000 km s^{-1} if the feature is Ca II. On October 9, the Ca II line close to the photosphere (at $-12{,}500$ km s^{-1}) becomes spectroscopically stronger than the high-velocity component. It is worth noting that no peculiar evolution of the polarization feature was observed to be associated with the emergence of the lower velocity Ca II feature.

In the *Q*-*U* plane the orientation, especially of the high-velocity feature, is at an angle of about 60° to the principal axis in the September 29 and October 1 data. This means that the high-velocity calcium represents a very distinct geometrical as well as velocity component in the explosion, with the difference in the orientation being about 30° in the object. Taken together, the velocity separation, the large amplitude of the polarization, and the different polarization angle all imply that this feature is a kinematically and geometrically separate high-velocity component that is enriched in calcium.

5. THE STRUCTURE OF THE SN 2001el EJECTA

The polarization evolution allows us to extract some useful information about the ejecta structure. For simplicity,

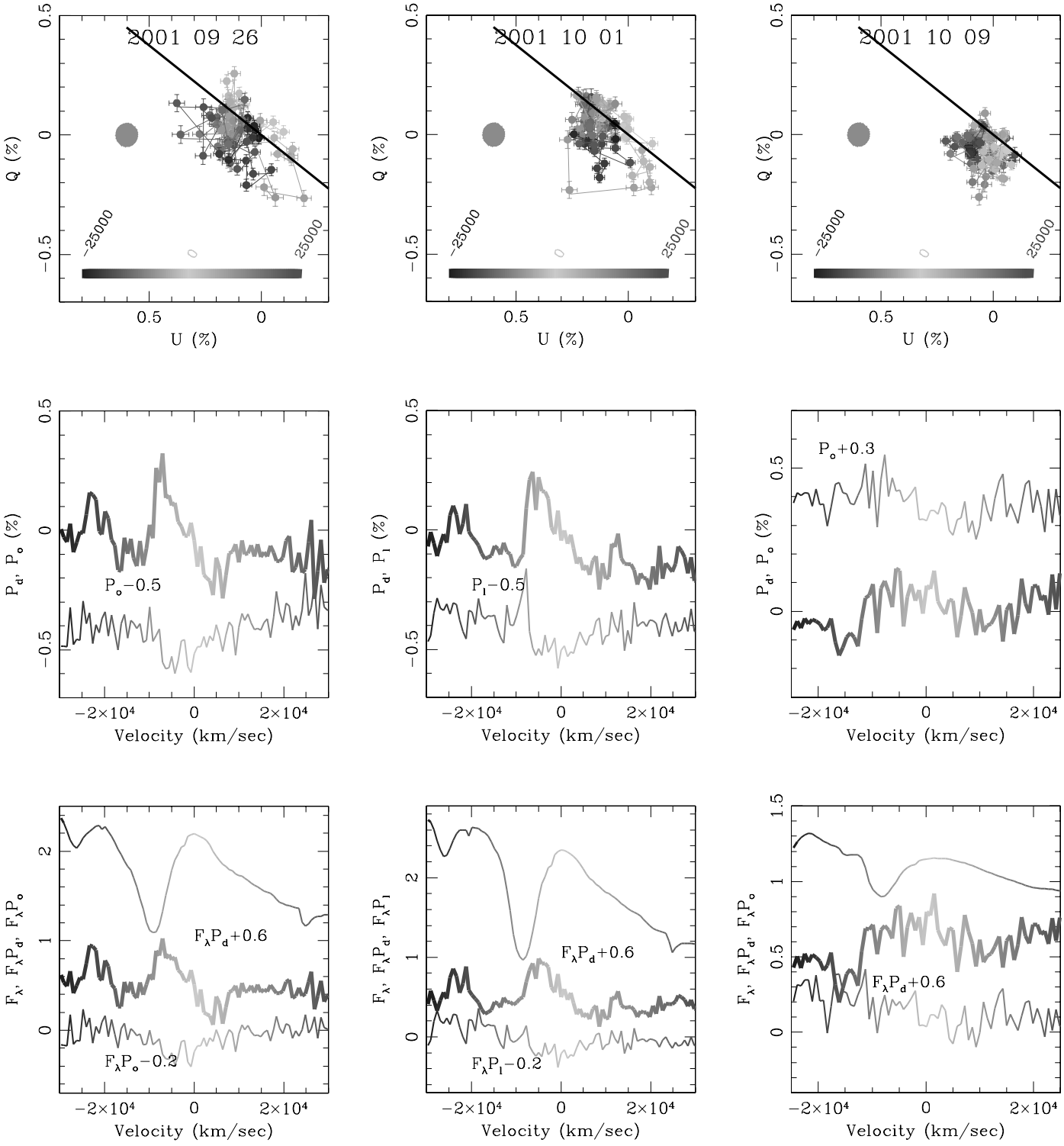

FIG. 10*a* FIG. 10*b* FIG. 10*c*

FIG. 10.—Evolution of polarization signatures of Si II 635.5 nm. The Si II 635.5 nm line shows conspicuous polarization on (*a*) September 26 and (*b*) October 1. The polarization signature weakened considerably for data taken on (*c*) October 9 and is undetected for data taken (*d*) October 18 and (*e*) November 11. [*See the electronic edition of the Journal for a color version of this figure.*]

we will assume that close to the photosphere the ejecta can be modeled as a prolate or oblate spheroid. We define the asphericity of the spheroid as the ratio of the major to minor axes minus 1, expressed as a percentage. This spheroid reproduces the dominant axis of asymmetry. The photosphere itself may be irregularly structured, so the spheroid is only an approximation. The relation between this geometric asymmetry and the angular distribution of the luminosity for an electron-scattering atmosphere is taken from Höflich (1991) and Wang, Wheeler, & Höflich (1997).

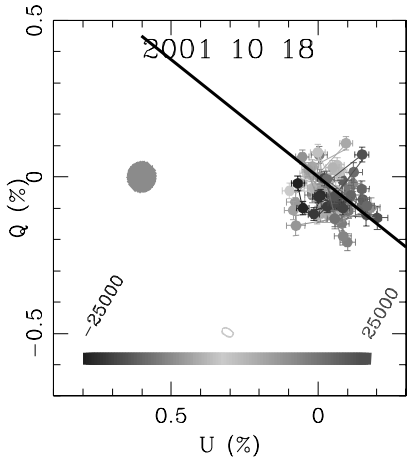

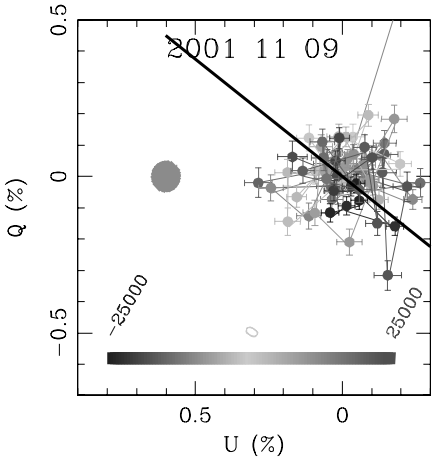

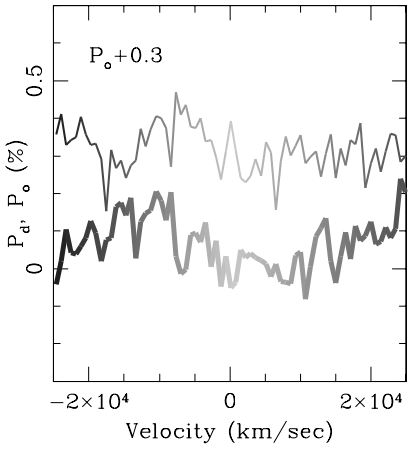

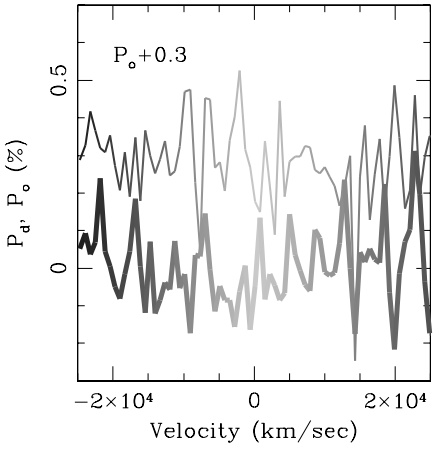

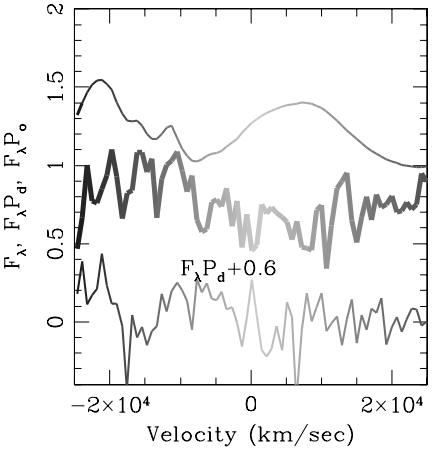

FIG. 10*d*

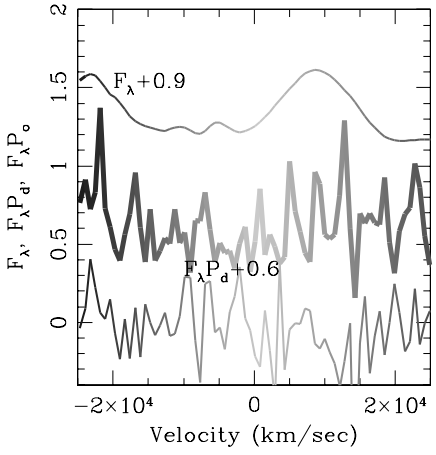

FIG. 10*e*

5.1. *Continuum Polarization*

For the maximum degree of polarization to be 0.7% on September 26 and October 1, an asphericity of 25% would be required for an ellipse observed along the equator (Höflich 1991; Howell et al. 2001). The 0.7% was, however, observed only for the 800 nm feature associated with the high-velocity Ca II IR triplet. If we think that the high-velocity component does not represent the global geometry of the photosphere, the maximum degree of polarization would be 0.2%–0.3% from the mean polarization spectrum on the dominant axis P_d shown in Figures 9*a*, 9*b*, and 9*c*. This is considerably smaller but would still require asymmetries around 10%–15% at the photosphere. The asphericity would be larger if the ellipsoid were viewed in a direction other than along the equator. This asymmetry could be pro-

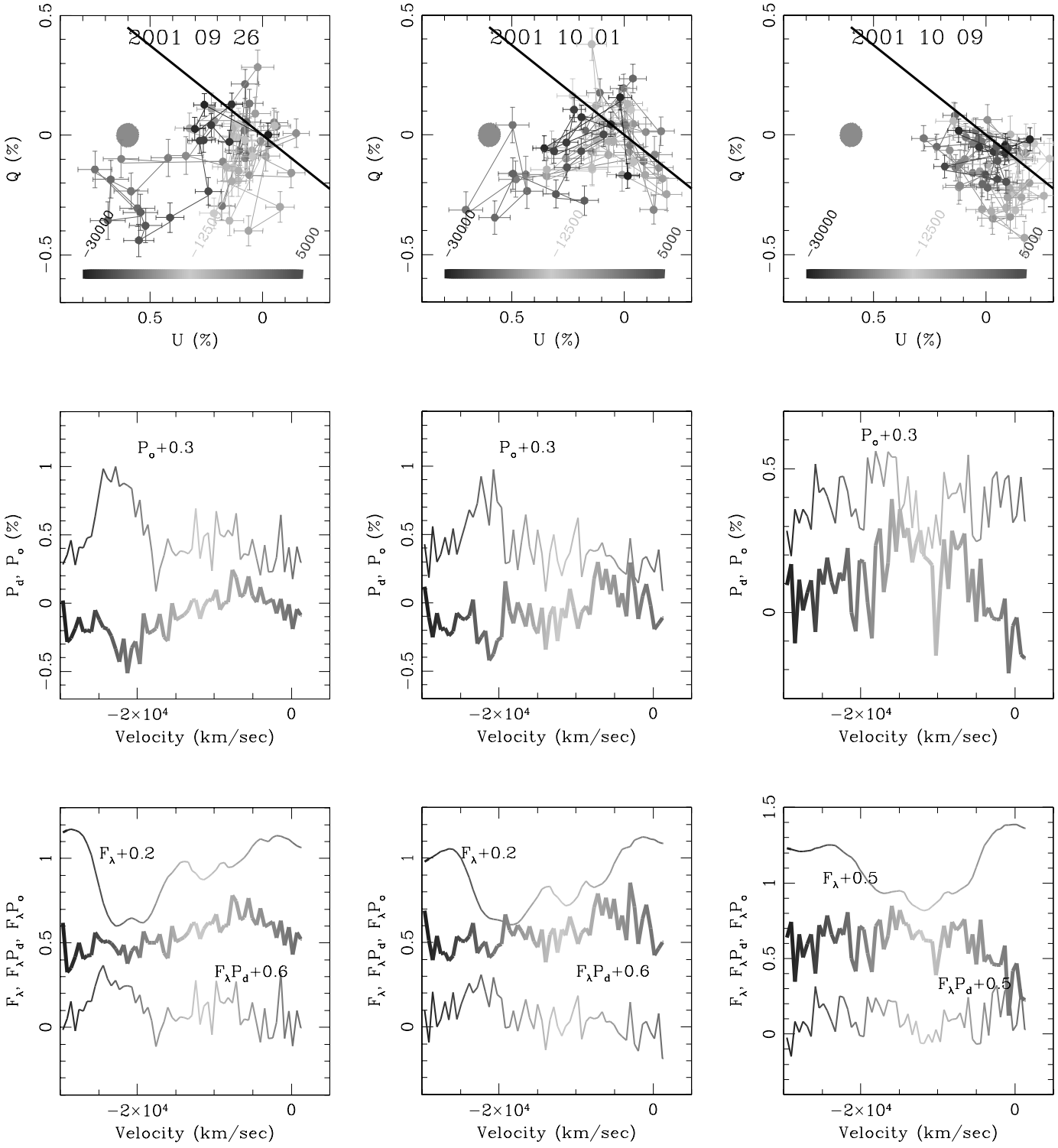

FIG. 11*a* FIG. 11*b* FIG. 11*c*

FIG. 11.—Evolution of the polarization signatures of the Ca II IR triplet. The velocities are calculated with respect to rest wavelength 860 nm. The Ca II IR triplet is polarized on (*a*) September 26 and (*b*) October 1. The strongest polarization is observed for the component with velocities around −25,000 and −20,000 km s^{-1}. The polarization signature weakened considerably for data taken on (*c*) October 9, (*d*) October 18, and (*e*) November 11. [*See the electronic edition of the Journal for a color version of this figure.*]

duced by a distortion in the density distribution or in the excitation by γ-ray deposition (Wang, Wheeler, & Höflich 1997; Howell et al. 2001; Höflich, Khokhlov & Wang 2001). This amount of asymmetry could lead to luminosity–viewing angle dependence with dispersion in brightness on the order of 0.1 mag even for otherwise identical events. We return to this possibility in § 7.

Small-scale inhomogeneities in the chemistry, density, or excitation must be present to account for the fact that the data points on the *Q-U* plot do not fall on a single line but

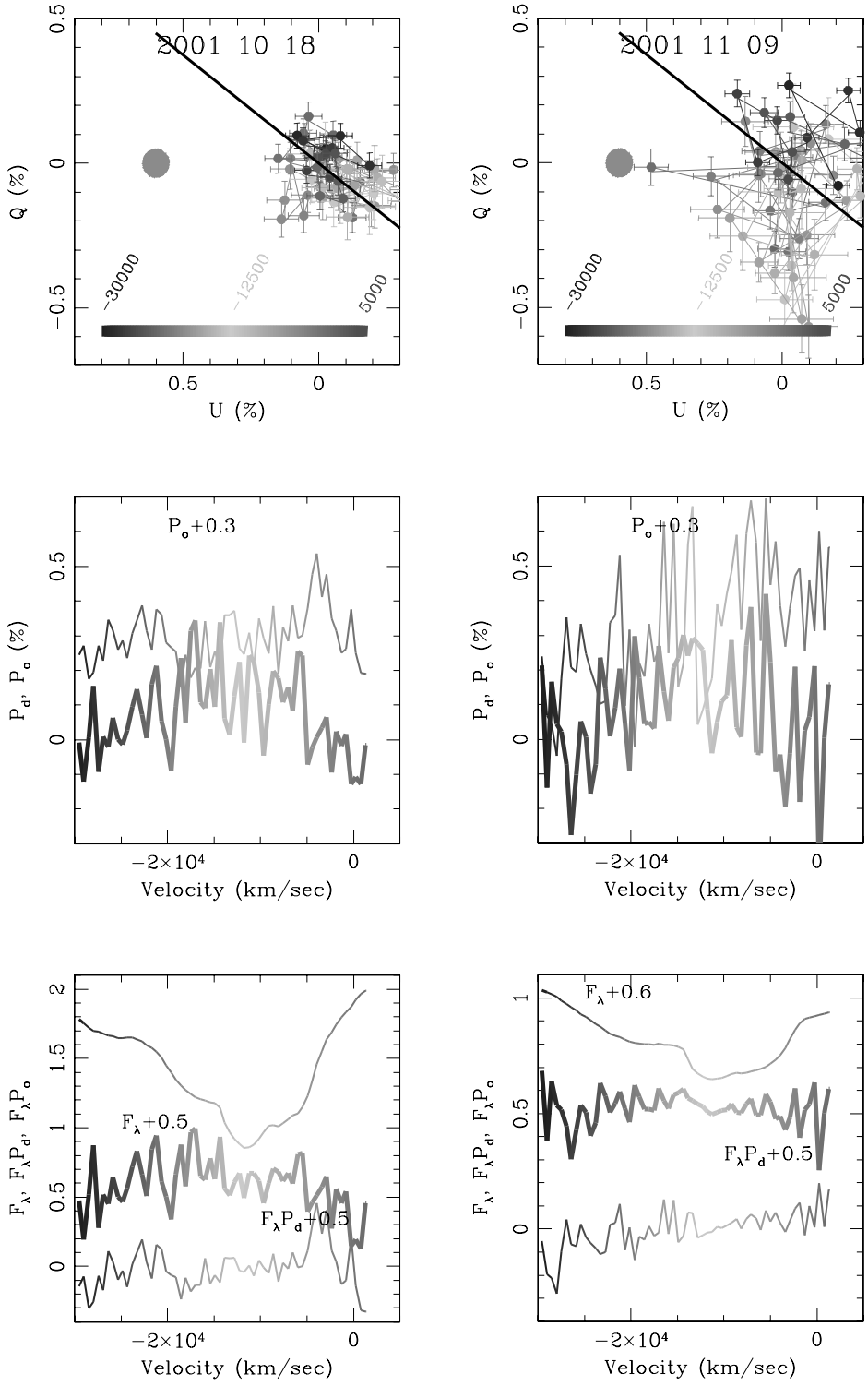

FIG. 11*d* FIG. 11*e*

show significant scatter around the dominant axis. Clumps of radioactive ^{56}Ni at the photosphere could produce these small-scale, random components as irregularities in the excitation. It would be interesting to try to model the number of clumps necessary to generate this granularity, but since the polarization represents a vector addition of the individual components, this is not a trivial exercise. We leave it for the future.

Further insight into this structure that deviates from the dominant axis may be obtained from the variation of the polarization angle with time and wavelength. With the adopted interstellar polarization, the principle component, P_d, changes sign with wavelength from blue to red in the premaximum spectra (see the first two panels of Fig. 9). A flip of the polarization vector can occur if the location of an energy source changes with respect to the photosphere. As

discussed for SN 1993J (Tran et al. 1997; Höflich 1995a), if the ^{56}Ni source is well below the photosphere, the flux is radial, but the flux acquires a tangential component if the energy source is close to the photosphere. This "skin effect" can cause a flip in the polarization angle. In 2001el, the flip of P_d with wavelength may be the result of such a skin effect in combination with the frequency-dependent opacity. In the blue, the photosphere is formed at much larger radii (by a factor of 2) compared to the red. If an excitation blob is buried in the blue but revealed in the red, the polarized flux will be determined by the radial and tangential flux, respectively, with an associated difference in the orientation of the polarization.

In SNe Ia, this flip of the sign of the polarization along the dominant axis might be due to a single large ^{56}Ni clump revealed at the photosphere in the red (Höflich 1995a). Such a single dominant blob would have to fall off the dominant geometric axis to produce the sign flip. Alternatively, there could be a distribution of a number of small blobs that are on average concentrated along the preferred axis. In this case the sign flip could occur when a number of these clumps are exposed, first in the red, by the receding photosphere. If this were the case, both the dominant polarization axis and the dispersion around it might be attributed to a common origin.

About 1–2 weeks after maximum light, the photosphere has receded well into the ^{56}Ni-rich region and, consequently, the effects of anisotropic excitation and ionization will vanish as the γ-ray deposition becomes smooth (Höflich et al. 2002). The polarization is then expected to become small, consistent with the observations (see Fig. 9*d*).

5.2. *Line Polarization*

The most dramatic aspect of the polarization of SN 2001el is the feature at 800 nm. This behavior of the Ca II IR triplet may provide a key to understanding the departure from axial symmetry. Among the possibilities to explain the strong high-velocity Ca II IR triplet in absorption at 22,000 km s^{-1} are a spherical shell; dense clumps, some of which fall along the line of sight; or a torus that intersects the line of sight to the photosphere of the supernova. As noted in § 3, the sharp edge to the photospheric component of the Ca II IR triplet implies that the density of Ca drops off beyond the photosphere before the high-velocity component is encountered. The high-velocity component is thus a distinct geometrical component, not simply a monotonic continuation of the calcium to high velocity in the ejecta.

As remarked in § 3, the high-velocity Ca II absorption line seems to be especially strong in SN 2001el. The strength in SN 2001el could be due to physical differences in this one event, but it could also be that this high-velocity feature is ubiquitous, that its presence is transient, and that its amplitude is sensitive to viewing angle. If the high-velocity Ca II is distributed aspherically in all SNe Ia, then SN 2001el may have just presented us with a lucky line of sight. There are relatively few cases in which observations have been made before maximum light, but in that situation, some evidence for a high-velocity feature is often seen, but evidence for a feature as strong and as disconnected in velocity space from the photospheric component as that in SN 2001el is, so far, unique to this event.

The existence and strength of the premaximum Ca II high-velocity component provides constraints on its physical nature. Whether the high-velocity Ca II component in SN 2001el is a single structure like a filament, a torus, dense clumps, or some other geometry, it could partially obscure the photosphere and make the photosphere appear asymmetric in the absorption lines. This would add another component to the polarization caused by an intrinsically aspherical photosphere. If this structure were an axially symmetric torus or a prominent filament, the axis of symmetry would have to be different from the symmetry axis of the photosphere to account for the orientation of the high-velocity calcium feature in the Q-U plane. If this component were caused by a calcium-rich clump, then the clump must be displaced from the principal axis. If the feature is caused by a distribution of calcium-rich clumps, then this distribution must deviate significantly from the dominant axis of the photosphere.

If the interpretation of the high-velocity component as a torus were correct, then, statistically, one would expect a correlation between the strength of the high-velocity absorption component and the size of its polarization. This would still be true for an asymmetric distribution of clumps, for instance if a surrounding torus were itself clumpy, but would not be true if the clumps responsible for obscuring the photosphere were themselves distributed isotropically around the explosion so there were no net effect of orientation angle.

The Si II 635.5 nm line falls predominantly along the P_d axis in the September 29 data (Fig. 9*a*) when the high-velocity Ca shows a distinct orientation along the P_o axis. The fact that in the Q-U plot, the Si II line also forms a "loop" on September 26 and October 1 shows that the Si II 635.5 nm line also cannot be explained only by an axially symmetric spheroid. The Si loop might show some preference to an orientation along the P_o axis in the October 1 data (Fig. 10*b*). This suggests that there might be a high-velocity Si counterpart to the high-velocity Ca, but the evidence is not conclusive; nevertheless, it is possible that the Si II line shares the same geometry as the Ca II line. If true, this would be an important constraint on the physical nature of the high-velocity feature.

6. PHYSICAL MODELS FOR ASYMMETRIES

How, then, might one account for a principle polarization axis of SN 2001el, the dispersion about that axis, and, especially, the detached, high-velocity feature seen so strongly in SN 2001el? Detailed modeling with three-dimensional radiative transfer is required to fully understand the polarization data (Höflich et al. 1996; Wang et al. 1997; Howell et al. 2001). This analysis will be presented elsewhere. Here we will discuss some of the physical possibilities.

As outlined in § 1, there are a variety of ways that systematic asymmetries could be imposed on the explosion of an SN Ia: rotation of the exploding star, an accretion disk, the presence of a binary companion, or plumes of combustion products. Some of these could define the dominant axis; others could account for varying orientation axes and still others for the dispersion observed around the dominant axis. Some affects of rotation have been sketched in Howell (2001), and we will not repeat them here. Marietta et al. (2000) show that the impact of the supernova ejecta with the secondary star, assumed to fill its Roche lobe, creates a hole in the ejecta with an angular size of $\sim 30^\circ$ in the high-velocity ejecta and with an angular size $\sim 40^\circ$ in the low-

velocity ejecta, or 7%–12% of the ejecta's surface. This effect might be able to induce the small photospheric polarization along the dominant axis that we report here, and it might not be observable in all SNe Ia because of orientation effects. We will return to the possible effects of an accretion disk below.

The greatest challenge in the current observations is to account for the high-velocity shell of calcium-rich material. The low-velocity Ca II seems to share the velocity, the degree of polarization, and the polarization angle with the photosphere. By contrast, the high-velocity matter defined by the 800 nm feature differs from the photosphere in velocity (by definition), in the degree of polarization, in the polarization angle, in the optical thickness, and in the filling factor. If the Ca II identification is correct, the high-velocity matter is physically and geometrically detached from the lower velocity material on the basis of the sharp edges of the absorption lines. The depth of the high-velocity feature requires that there must be two zones of Ca II. These zones differ by so much in geometry, dynamics, and column density that it is difficult to accommodate them in an exploding star of only one component. The impressive homogeneity of SNe Ia does not leave much room for major individual peculiarities. This is an additional constraint every model of SN 2001el needs to satisfy. We will sketch here and critique several possibilities.

6.1. *The Mass of High-Velocity Ejecta*

In order to make a high-velocity shell of calcium-rich material modestly optically thick so that it can obscure a patch of the photosphere and induce a significant polarization feature, there must be a substantial mass of high-velocity calcium. A simple static atmosphere argument suggests the following. Taking an effective opacity of order 1 $\mathrm{cm^2\ g^{-1}}$ and shell radius and thickness of order 10^{15} cm, the mass of calcium must be of order $5 \times 10^{-3} f \kappa^{-1} R_{15}^2\ M_\odot$ to give an optical depth of order unity, where f is the filling factor of the high-velocity shell.

A more rigorous approach is to consider the Sobolev optical depth of the line:

$$\tau = \chi c \rho \frac{dr}{dv} , \tag{3}$$

where $dr/dv = t$ in a homologously expanding atmosphere and χ is the integrated line opacity given by

$$\chi = \frac{\pi e^2}{m_e c} \frac{f_{ul} n_l}{\nu_{ul} \rho} \left(1 - \frac{g_l n_u}{g_u n_l}\right) , \tag{4}$$

where f_{ul} and ν_{ul} are the oscillator strength and frequency for the line that represents a transition from the lower (l) to upper (u) levels. Neglecting the second term in parentheses involving the statistical weights and writing the population in the lower level as $n_l = n_{\mathrm{Ca}} \exp(-E_l/kt)$, where n_{Ca} is the total number of calcium atoms, the Sobolev optical depth can be written as

$$\tau = \frac{\pi e^2}{m_e c} f_{ul} n_{\mathrm{Ca}} \lambda_{ul} t e^{-E_l/kt} , \tag{5}$$

where E_l is the energy of the lower level. With $f_{ul} \sim 3$, $E_l = 60,533\ \mathrm{cm^{-1}} = 1.2 \times 10^{-11}$ ergs, and a temperature of about 5000 K, the Sobolev optical depth can be written as

$$\tau = 2.6 \times 10^{15} \rho_{\mathrm{Ca}} t_6 , \tag{6}$$

where t_6 is the time in units of 10^6 s. The mass of calcium in a spherical shell with filling factor f can thus be written

$$M_{\mathrm{Ca}} = 0.002\ M_\odot \frac{f \tau R_{15}^2 \Delta R_{15}}{t_6} . \tag{7}$$

For a putative Ca line at 20,000 km $\mathrm{s^{-1}}$ with a width of $\sim$5000 km $\mathrm{s^{-1}}$, the mass of calcium would thus be $M_{\mathrm{Ca}} = 0.004 f \tau t_6^2\ M_\odot$. For optical depth about unity and filling factor of unity, we again need of order 0.01 $M_\odot$ of calcium to form the high-velocity feature.

In regions of the WD where Ca is formed by incomplete Si burning, the layers are typically 60% Si, 30% S, and 3% Ca (Höflich et al. 2002). If this composition is typical of the high-velocity shell, then the total mass of this matter might be of order $0.1 f \tau t_6^2\ M_\odot$. As remarked earlier, if the paucity of this strong, well-separated feature in many SNe Ia is an indication of the covering factor, then f could be substantially less than unity. Given the relative strengths of observable lines, it is plausible that the Ca would give the strongest observed line, with Si weak and S difficult to observe, as may be the case for SN 2001el.

6.2. *The Geometry of High-Velocity Ejecta*

A related perspective is to consider the shape and depth of the high-velocity feature. The feature is approximately flat bottomed (ignoring the double minimum in the September 26 spectrum of Fig. 2). This suggests that the line is optically thick over a substantial velocity range. The line should thus be saturated if the feature obscured the whole photosphere. From the depth of the line (about 30% of the adjacent continuum flux), we deduce that the geometry can be blocking no more than about 30° of the photosphere. Note that if the high-velocity component extended to higher latitudes, there should be a low-velocity component along the line of sight. The rather sharp edges of the high-velocity feature and its lack of overlap with the photospheric component of the Ca II IR triplet again suggest that the portion of this high-velocity feature with finite optical depth does not blanket the photosphere. Some sort of torus geometry could satisfy this constraint. To account for what may be common weaker high-velocity features in SNe Ia, some of the high-velocity calcium may have to be distributed more isotropically but with modest optical depth. If this component is present in SN 2001el, then it must be in a manner that low-velocity wings on the high-velocity feature are weak. Whether a self-consistent model can be developed will require more rigorous consideration with multidimensional transfer.

6.3. *The Origin of High-Velocity Ejecta*

One possibility is that this high-velocity matter is produced in the explosion in the region of partial Si burning. In this case, a stream of matter must be ejected from relatively deep within the explosion as, perhaps, a filament of high-velocity matter. This might happen through some sort of "pinch" effect. A particularly interesting possibility is that this high-velocity feature represents an artifact of the process of deflagration to detonation transition. The physics of this process is not yet well understood, but one possibility

being explored is that the transition occurs between a rising plume of burned material and a sinking plume of fuel. Ignition of a detonation at the sheetlike interface between these structures might, in some circumstances, dynamically eject a ballistic blob of matter that was subject to partial Si burning. The hint that some silicon may share the high-velocity kinematics of the calcium would be consistent with the composition expected in this picture. If this were the case, the high-velocity feature would be an important clue to the burning dynamics.

Another intriguing possibility is that the high-velocity matter is a clue to the binary nature of the progenitor. In particular, it is clear that any matter in an accretion disk should be swept up into a high-velocity layer, possibly maintaining a toroidal structure. The question then arises as to how this matter could be calcium-rich.

The most commonly envisaged scenario would have a hydrogen-rich disk. The collision of the most rapidly moving outer parts of the WD ejecta, exceeding 10,000 km s^{-1}, would heat any such disk to high temperatures. If the postshock conditions were optically thick and dominated by radiation pressure, the temperature would be of order 1.2×10^8 K $\rho^{1/4} v_9^{1/2}$, where v_9 is the shock velocity in units of 10^9 cm s^{-1}. If the postshock matter can radiate so that the shock energy goes into purely the thermal motion of particles, then the temperature could be as high as $4 \times 10^9 v_9^2$ K. The density is expected to be low, less than 1 g cm^{-3}, so while the postshock temperature could be sufficiently high that burning might occur, the burning timescale could be too long compared to the dynamical timescale, which will be of order 1 s at the inner edge of the disk at the boundary with the WD. If it occurs, the burning in this hydrogen-rich situation would correspond to the fast rp-process (Wallace & Woosley 1981). Burning would break out of the CNO cycle at this high temperature and proceed to higher atomic weight matter. The resulting composition may not be calcium-rich but dominated by more neutron rich species.

Another interesting possibility is that the disk is composed of helium, the product of transfer from a helium star. Such a disk might be denser, depending on the temperature and transfer rate (Cannizzo 1984), and the composition would allow burning along the standard α-chain with the possible production of Ca, along with Si and S, through incomplete Si burning. While it is clearly premature to reach any conclusions regarding the nature of this high-velocity Ca feature, the prospect that it represents the shock burning of a helium-rich accretion disk would give direct indications both that the explosion occurred in a binary system and that a helium, not hydrogen, companion was involved.

7. DISCUSSION AND CONCLUSIONS

Understanding the three-dimensional nature of SNe Ia is an important key to the underlying physics, and polarimetry is the tool to probe multidimensional effects.

The current observations provide strong evidence that the normal Type Ia SN 2001el is polarized before optical maximum. The polarization cannot be explained by a purely axially symmetric configuration; rather, several components are required, as follows. (1) An axially symmetric component with polarization of about 0.2%–0.3% with a well-defined axis: this component indicates that the overall asphericity of the photosphere is around 10% and perhaps more, depending on viewing angle. This global asymmetry may either be produced by asymmetric excitation and ionization or it may reflect asymmetry in the overall density distribution. (2) A component to account for the spread in the position angle with wavelength around the principal axis in the Q-U plane that indicates additional structure with more random orientation: this component could be caused by clumps in the chemical structure. If the clumps are related to the ^{56}Ni distribution, they could be related to irregularities in the excitation expected from the RT instabilities during the deflagration phase of the explosion (Khokhlov 2002). (3) The high degree of polarization in the high-velocity component of the Ca II IR triplet: this component, which is at an angle of about 60° to the principal axis in the Q-U plane, can be understood qualitatively as an obscuration of a portion of the photosphere by a filament, clumps, or perhaps a torus-like structure expanding at high velocity. The sharp blue edge of the photospheric component of the Ca II IR triplet and the relatively sharp red edge of the high-velocity component indicate the origin of the high-velocity component in a separate structure well separated from the photosphere. The fact that the line is not saturated suggests that the filling factor is substantially less than unity.

Excitation due to the nonuniform distribution of ^{56}Ni provides a natural explanation for observations of the photospheric polarization, and hence clues to the burning process, but other explanations are possible. The merger scenario, would, for instance, predict a global asymmetry due to the large expected rotation of the merged object. The merger scenario is not likely for SN 1994D, which showed evidence for explosive carbon burning in the outer layers (i.e., IR Mg II lines), but no evidence for unburned carbon (Bowers et al. 1997; Wheeler et al. 1998) as would be expected in a merger scenario. Since SN 2001el is in many ways similar to SN 1994D, a similar argument might be applied, but the IR observations were not made. It may be that detailed analysis and models can address this issue from the polarization and other data at hand for SN 2001el.

The polarization data provide interesting perspectives on the physics of SN Ia phenomena, but there are many open questions. What is the origin of the high-velocity Ca II in SN 2001el? Could the Ca II shell be the relic of an accretion disk? If so, what is the composition of the accretion disk and could it be burned into Ca? We will focus on these issues in separate studies incorporating detailed theoretical modeling. The model-dependent interpretations of the high-velocity Ca II feature could be put on a much firmer basis if future observations confirm (1) a correlation between the strength and the degree of polarization of the Ca II IR triplet, (2) the $\sim$30° difference in the polarization angle of the continuum and of the high-velocity matter, and (3) a correlation between the polarization of the continuum and the polarization of the high-velocity Ca II, presuming their respective dominant axes are defined by the equator and the rotation or magnetic axis.

Finally, we return to the implications of asymmetry for the use of SNe Ia for cosmology. A 10% asymmetry of the photosphere would not cause systematic difficulties for using SNe Ia as distance indicators at the current level of accuracy of about 20%. This level of asymmetry would, however, cause a directional dependence of the luminosity of order 0.1 mag (Höflich 1991) and a corresponding, but smaller, dispersion in the brightness-decline relation of SNe Ia. This dispersion depends on the viewing angle dependence of the luminosity variation and, thus, the nature of the

asymmetry. The angle dependence of the luminosity of a single SN Ia will not, in general, vary as the line of sight to the equator, that is, as $\cos\theta$. Thus, even in a large sample, this effect is not expected to average out. Whether the remaining bias is slightly positive or slightly negative depends on the specifics of the asymmetric luminosity distribution. Whether this bias can be eliminated to the few percent level needed to determine the cosmological equation of state by applying the ΔM_{15} correction or by employing the CMAGIC method (Wang et al. 2003) remains to be seen. We note that if such effects are present, then SNe Ia are even more homogeneous than they seem from current dispersions in peak brightness. In principle, if the angle-dependent luminosity could be determined and removed quadratically from the data, the dispersion could be reduced from current values.

More observations are required to understand the polarization behavior of SNe Ia and its effect on large samples of supernovae. Once we know from polarization statistics the phases in which the polarization is small, more weight can be assigned to the "low-risk" phases of the light curve. Even if there remains a bias due to the angle dependence of the emitted flux, this may have no affect in a large sample as long as the bias is independent of redshift. The relative changes in peak magnitude with redshift that are required to determine the equation of state of the "dark energy" would not be affected by such a constant bias. Even then a redshift-dependent bias might be small if the only effect were that of an ellipsoidal variation of rather small amplitude for which the luminosity variation with angle were small and gentle. The pernicious question is whether there is an effect on the polarization and hence luminosity distribution that was a rather strong function of observer orientation and that also depended on redshift. An example would be polarization induced by the collision of the supernova ejecta with a companion star that might be seen only from a limited range of observer viewing angles coupled with SNe Ia being dominated nearby by SNe Ia in systems with nondegenerate companions and at large redshifts by mergers that left no companion, or vice versa. Further study of the polarization of SNe Ia should elucidate this issue.

The authors are grateful to the European Southern Observatory for the generous allocation of observing time. They especially thank the staff of the Paranal Observatory for their constant and untiring support of this project in service mode. This work was supported in part by NASA grant NAG5-7937 to P. A. H. and by NSF grant AST 00-98644 to J. C. W.

REFERENCES

Albrecht, A., & Weller, J. 2000, BAAS, 197, 61.06
Böhnhardt, H., & Szeifert, T. 2002, FORS1+2 User Manual, Revision 2.3 (Garching: ESO)
Bowers, E. J. C., Meikle, W. P. S., Geballe, T. R., Walton, N. A., Pinto, P. A., Dhillon, V. S., Howell, S. B., & Harrop-Allin, M. K. 1997, MNRAS, 290, 663
Cannizzo, J. K. 1984, Nature, 311, 443
Domínguez, I., Höflich, P., & Straniero, O. 2001, ApJ, 557, 279
Gamezo, V. N., Wheeler, J. C., Khokhlov, A. M., & Oran, E. S. 1999, ApJ, 512, 827
Hamuy, M., Phillips, M. M., Suntzeff, N. B., Schommer, R. A., Maza, J., & Aviles, R. 1996, AJ, 112, 2398
Hatano, K., Branch, D., Fisher, A., Baron, E., & Filippenko, A. V. 1999, ApJ, 525, 881
Höflich, P. 1991, A&A, 246, 481
———. 1995a, ApJ, 440, 821
———. 1995b, ApJ, 443, 89
Höflich, P., Gerardy, C. L., Fesen, R. A., & Sakai, S. 2002, ApJ, 568, 791
Höflich, P., & Khokhlov, A. 1996, ApJ, 457, 500
Höflich, P., Khokhlov, A. M., & Wang, L. 2001, in AIP Conf. Proc. 586, 20th Texas Symp. on Relativistic Astrophysics, ed. J. C. Wheeler & H. Martel (Melville: AIP), 459
Höflich, P., & Stein, J. 2002, ApJ, 568, 779
Höflich, P., Wheeler, J. C., Hines, D. C., & Trammell, S. R. 1996, ApJ, 459, 307
Höflich, P., Wheeler, J. C., & Thielemann, F. K. 1998, ApJ, 495, 617
Howell, D. A. 2001, ApJ, 554, L193
Howell, D. A., Höflich, P., Wang, L., & Wheeler, J. C. 2001, ApJ, 556, 302
Hoyle, F., & Fowler, W. A. 1960, ApJ, 132, 565
Iben, I. J., & Tutukov, A. V. 1984, ApJS, 54, 335
Iwamoto, K., Brachwitz, F., Nomoto, K., Kishimoto, N., Umeda, H., Hix, W. R., & Thielemann, F. 1999, ApJS, 125, 439
Jeffrey, D. J. 1991, ApJ, 375, 264
Kasen, D., et al. 2003, ApJ, in press
Khokhlov, A. M. 1991, A&A, 245, 114
———. 1995, ApJ, 449, 695
———. 2002, preprint (astro-ph/0008463)
Krisciunas, K., et al. 2003, AJ, 125, 166
Langer, N., Deutschmann, A., Wellstein, S., & Höflich, P. 2000, A&A, 362, 1046
Larson, K. A., Whittet, D. C. B., & Hough, J. H. 1996, ApJ, 472, 755
Lentz, E. J., Baron, E., Branch, D., & Hauschildt, P. H. 2001, ApJ, 547, 402
Leonard, D. C., & Filippenko, A. V. 2001, PASP, 113, 920
Leonard, D. C., Filippenko, A. V., Ardila, D. R., & Brotherton, M. S. 2001, ApJ, 553, 861
Leonard, D. C., Filippenko, A. V., Barth, A. J., & Matheson, T. 2000, ApJ, 536, 239
Livne, E. 1993, ApJ, 406, L17
Livne, E., Tuchman, Y., & Wheeler, J. C. 1992, ApJ, 399, 665
Marietta, E., Burrows, A., & Fryxell, B. 2000, ApJS, 128, 615
Monard, L. A. G. 2001, IAU Circ. 7720
Nomoto, K. 1982, ApJ, 257, 780
Nomoto, K., Sugimoto, D., & Neo, S. 1976, Ap&SS, 39, L37
Nomoto, K., Thielemann, F.-K., & Yokoi, K. 1984, ApJ, 286, 644
Nugent, P., Baron, E., Branch, D., Fisher, A., & Hauschildt, P. H. 1997, ApJ, 485, 812
Paczyński, B. 1985, in Cataclysmic Variables and Low-Mass X-Ray Binaries, ed. D. Q. Lamb & J. Patterson (Dordrecht: Reidel), 1
Perlmutter, S., Turner, M. S., & White, M. 1999, Phys. Rev. Lett., 83, 670
Perlmutter, S., et al. 1997, ApJ, 483, 565
Reinecke, M., Hillebrandt, W., & Niemeyer, J. C. 1999, A&A, 347, 739
Riess, A. G., Press, W. H., & Kirshner, R. P. 1996, ApJ, 473, 88
Riess, A. G., et al. 1998, AJ, 116, 1009
Schlegel, D. J., Finkbeiner, D. P., & Davis, M. 1998, ApJ, 500, 525
Serkowski, K., Mathewson, D. L., & Ford, V. L. 1975, ApJ, 196, 261
Sharpe, G. J. 2001, MNRAS, 322, 614
Sollerman, J., Leibundgut, B., & Lundqvist, P. 2001, IAU Circ., 7723, 2
Tody, D. 1993, in ASP Conf. Ser. 52, Astronomical Data Analysis Software and Systems II, ed. R. J. Hanisch, R. J. V. Brissenden, & J. Barnes (San Francisco: ASP), 173
Trammell, S. R., Hines, D. C., & Wheeler, J. C. 1993, ApJ, 414, L21
Tran, H. D., Filippenko, A. V., Schmidt, G. D., Bjorkman, K. S., Jannuzi, B. T., & Smith, P. S. 1997, PASP, 109, 489
Wallace, R. K., & Woosley, S. E. 1981, ApJS, 45, 389
Wang, L., Goldhaber, G., Aldering, G., & Perlmutter, S. 2003, ApJ, in press
Wang, L., Howell, D. A., Höflich, P., & Wheeler, J. C. 2001a, ApJ, 550, 1030
Wang, L., Wheeler, J. C., & Höflich, P. 1997, ApJ, 476, L27
Wang, L., Wheeler, J. C., Li, Z., & Clocchiatti, A. 1996, ApJ, 467, 435
Wang, L., et al. 2001b, IAU Circ., 7724, 2
Weaver, T. A., Axelrod, T. S., & Woosley, S. E. 1980, in Type I Supernovae: Proc. Texas Workshop, ed. J. C. Wheeler (Austin: Univ. Texas), 113
Webbink, R. F. 1984, ApJ, 277, 355
Weller, J., & Albrecht, A. 2002, Phys. Rev. D, 65, 3512
Wheeler, J. C., Höflich, P., Harkness, R. P., & Spyromilio, J. 1998, ApJ, 496, 908
Whelan, J., & Iben, I., Jr. 1973, ApJ, 186, 1007
Whittet, D. C. B., Gerakines, P. A., Hough, J. H., & Shenoy, S. S. 2001, ApJ, 547, 872
Wilking, B. A., Lebofsky, M. J., & Rieke, G. H. 1982, AJ, 87, 695
Woosley, S. E., & Weaver, T. A. 1986, ARA&A, 24, 205
Yamaoka, H., Nomoto, K., Shigeyama, T., & Thielemann, F. 1992, ApJ, 393, L55